PFC/JA-85-40

INFLUENCE OF INTENSE EQUILIBRIUM SELF FIELDS ON THE CYCLOTRON MASER INSTABILITY IN HIGH-CURRENT GYROTRONS

Han S. Uhm
and
Ronald C. Davidson

October, 1985

Submitted for publication in: The Physics of Fluids

TABLE OF CONTENTS

ABSTRACT

The linearized Vlasov-Maxwell equations are used to investigate the influence of intense equilibrium self fields on the cyclotron maser instability. A uniform density ($\hat{n}_b$) electron beam propagates parallel to an applied axial magnetic field $B_0\hat{e}_z$ with average axial velocity $\beta_b c$. The particle trajectories are calculated including the influence of the radial self-electric field and the azimuthal self-magnetic field. Moreover, the linearized Vlasov-Maxwell equations are analyzed for body-wave perturbations localized to the beam interior, assuming electromagnetic perturbations about the equilibrium distribution function $f_b^0 = (\hat{n}_b/2\pi p_\perp) \times \delta(p_\perp - \gamma_b m V_\perp)\delta(p_z - \gamma_b m \beta_b c)$. Near the beam axis ($\omega_{pb}^2 r^2/c^2 << 1$), it is found that the transverse electron motion is biharmonic, with oscillatory components at the frequencies ω_b^+ and ω_b^- defined by $\omega_b^\pm = (\omega_{cb}/2)\left\{1 - [1 - (2\omega_{pb}^2/\omega_{cb}^2)(1-\beta_b^2)]^{\frac{1}{2}}\right\}$. Similarly, the electromagnetic dispersion relation for waves propagating parallel to $B_0\hat{e}_z$ exhibits two types of resonance conditions: a high frequency resonance (HFR) corresponding to $\omega - k\beta_b c = \omega_b^+$, and a low frequency resonance (LFR) corresponding to $\omega - k\beta_b c = \omega_b^-$. Both the HFR branch and the LFR branch exhibit instability, with detailed stability properties depending on the value of the self-field parameter $s = \omega_{pb}^2/\omega_{cb}^2$. Moreover, the LFR branch is entirely due to self-field effects, whereas the HFR branch represents a generalization of the conventional cyclotron maser mode to include self-field effects. The full dispersion relation is analyzed numerically, and the real oscillation frequency $\omega_r = \mathrm{Re}\omega$ and growth rate $\omega_i = \mathrm{Im}\omega$ are calculated for both types of modes over a wide range of system parameters s, $\beta_\perp$, β_b and kc/ω_{cb}. Analytic estimates are made of the cyclotron maser growth properties in circumstances where $\beta_\perp^2\gamma_z^2/2$ is treated as a small parameter. [Here, $\gamma_z = (1-\beta_b^2)^{-\frac{1}{2}}$.] It is found that the maximum growth rate is given by $\omega_i = (2\gamma_z^2)^{-1}[s(2\beta_\perp^2\gamma_z^4 - s)]^{\frac{1}{2}}\omega_{cb}$, which occurs for wavenumber $k = k_m = \gamma_z^2\beta_b\omega_{cb}/c$. As the beam density ($s$) is increased, the growth rate ω_i increases to the maximum value $\omega_i^{max} = \gamma_z^2\beta_\perp^2\omega_{cb}/2$ for beam density $s = s_m = \beta_\perp^2\gamma_z^4$. As s is increased beyond s_m, the growth rate ω_i decreases to zero for $s = s_0 = 2\beta_\perp^2\gamma_z^4$. Similarly, the instability bandwidth $\Delta k = (2\gamma_z\omega_{cb}/c)[\gamma_z^2 - \beta_\perp^{-1}(s/2)^{\frac{1}{2}}]^{\frac{1}{2}}$ approaches zero as s approaches s_0.

I. INTRODUCTION AND SUMMARY

There is growing experimental[1-3] and theoretical[4-9] evidence that the cyclotron maser instability is an effective mechanism for coherent radiation generation by intense electron beams. For the most part, gyrotron devices have been operated at relatively low current, where equilibrium self-field effects are negligibly small. However, with the increasing interest in high-power gyrotron applications, it is important to investigate properties of the cyclotron maser instability under conditions corresponding to high beam current and density. For sufficiently high beam density, as measured by the dimensionless parameter[10,11]

$$s = \frac{\omega_{pb}^2}{\omega_{cb}^2} ,$$

it is anticipated that equilibrium self fields will have a large influence on detailed stability properties. Here, $\omega_{cb} = eB_0/\gamma_b mc$ is the relativistic cyclotron frequency, $\omega_{pb}^2 = 4\pi\hat{n}_b e^2/\gamma_b m$ is the relativistic plasma frequency-squared, $\hat{n}_b$ is the electron density, $\gamma_b mc^2$ is the characteristic electron energy, and B_0 is the strength of the axial magnetic field. Previous theoretical studies of the cyclotron maser instability[4-9,12,13] have assumed $s \ll 1$. However, a recent calculation by Davidson and McMullin[10] shows that the spontaneous emission by a test electron in a nonneutral electron beam is significantly modified by equilibrium self-field effects at moderate values of the parameter s. The purpose of the present analysis is to develop a kinetic description of the cyclotron maser instability which includes the influence of equilibirum self fields in a self-consistent manner.

The equilibrium configuration and particle trajectories are discussed in Sec. II. A uniform density ($\hat{n}_b$) electron beam propagates parallel

to the applied magnetic field $B_0\hat{e}_z$ with average axial velocity $\beta_b c$. Within the electron beam ($r<r_b$), the particle trajectories are calculated in Sec. II including the influence of the radial self-electric field $\underset{\sim}{E}_0^s(\underset{\sim}{x})$ and azimuthal self-magnetic field $\underset{\sim}{B}_0^s(\underset{\sim}{x})$ [Eq.(7)]. Near the beam axis ($\omega_{pb}^2 r^2/c^2 << 1$), it is found that the electron motion transverse to $B_0\hat{e}_z$ is biharmonic with oscillatory components at the frequencies ω_+ and ω_- defined in Eq.(19). For electron energy γmc^2 strongly peaked around $\gamma \simeq \gamma_b$ = const., and axial velocity $\beta_z c$ strongly peaked around $\beta_z \simeq \beta_b$ = const., the frequencies $\omega_\pm$ [Eq.(19)] reduce to $\omega_b^\pm$ defined by [Eq.(37)]

$$\omega_b^\pm = \frac{\omega_{cb}}{2}\left\{1 \pm \left[1 - \frac{2\omega_{pb}^2}{\omega_{cb}^2}(1-\beta_b^2)\right]^{\frac{1}{2}}\right\} .$$

For negligibly small equilibrium self fields, the inequality $(2\omega_{pb}^2/\omega_{cb}^2)(1-\beta_b^2) << 1$ pertains, and Eq.(37) reduces to $\omega_b^+ \to \omega_{cb}$ and $\omega_b^- \to 0$.

In Sec. III, including equilibrium self-field effects, the linearized Vlasov-Maxwell equations are used to investigate electromagnetic stability properties for body-wave perturbations localized to the beam interior. Neglecting transverse spatial variations ($\partial/\partial x = 0 = \partial/\partial y$), and assuming perturbations about the uniform beam equilibrium [Eq.(6)]

$$f_b^0(p_\perp^2, p_z) = \frac{\hat{n}_b}{2\pi p_\perp}\,\delta(p_\perp - \gamma_b m V_\perp)\,\delta(p_z - \gamma_b m \beta_b c) ,$$

the resulting dispersion relation for right-circularly-polarized electromagnetic waves propagating parallel to $B_0\hat{e}_z$ is given by [Eq.(36)]

$$\frac{\omega^2}{c^2} - k^2 = \frac{\omega_{pb}^2}{c^2} \frac{(\omega-k\beta_b c)^2}{(\omega-k\beta_b c)^2 - \omega_{cb}(\omega-k\beta_b c) + \omega_{pb}^2(1-\beta_b^2)/2}$$

$$- \frac{\omega_{pb}^2}{2c^2} \beta_\perp^2 \frac{(\omega^2-k^2c^2)[(\omega-k\beta_b c)^2 - (\omega_{pb}^2/2)(1-\beta_b^2)] + (\omega-k\beta_b c)^2(\omega_{pb}^2/2)}{[(\omega-k\beta_b c)^2 - \omega_{cb}(\omega-k\beta_b c) + (\omega_{pb}^2/2)(1-\beta_b^2)]^2}$$

Here, $\beta_\perp = V_\perp/c$, k is the axial wavenumber, and ω is the (complex) oscillation frequency with $\mathrm{Im}\omega > 0$ corresponding to instability. In the limit of a tenuous electron beam with $(2\omega_{pb}^2/\omega_{cb}^2)(1-\beta_b^2) \ll 1$, Eq.(36) reduces to the familiar dispersion relation[12,13] for the cyclotron maser instability, which exhibits resonant behavior when the cyclotron resonance condition $\omega-k\beta_b c = \omega_{cb}$ is satisfied. However, for finite, non-zero values of $(2\omega_{pb}^2/\omega_{cb}^2)(1-\beta_b^2)$, it is found that the dispersion relation exhibits two types of resonances. These are: a <u>high frequency resonance</u> (HFR) corresponding to [Eq.(41)]

$$\omega-k\beta_b c = \omega_b^+ ,$$

and a <u>low frequency resonance</u> (LFR) corresponding to [Eq.(42)]

$$\omega-k\beta_b c = \omega_b^- .$$

The high frequency condition $\omega-k\beta_b c = \omega_b^+$ is a generalization of the cyclotron resonance condition $\omega-k\beta_b c = \omega_{cb}$ to include equilibrium self-field effects. The low frequency resonance condition $\omega-k\beta_b c = \omega_b^-$ is new and is entirely associated with self-field effects.

In Sec. IV, the dispersion relation (36) is solved numerically for the real oscillation frequency $\omega_r = \mathrm{Re}\omega$ and growth rate $\omega_i = \mathrm{Im}\omega$ over a wide range of system parameters $s = \omega_{pb}^2/\omega_{cb}^2$, $\beta_\perp$, β_b and kc/ω_{cb}. It is

found that both the HFR branch and the LFR branch exhibit instability. Moreover, detailed stability properties are strongly affected by the equilibrium self fields, even at relatively modest values of $s(\gtrsim 0.1)$. While the majority of the unstable LFR branch corresponds to slow-wave propagation ($|\omega_r/k| < c$), it is found that the HFR branch corresponds primarily to fast-wave propagation ($|\omega_r/k| > c$) with $\omega_r - k\beta_b c \simeq \omega_{cb}$ for a wide range of system parameters. This mode is identified with the cyclotron maser instability, appropriately modified by equilibrium self-field effects. In Sec. V, the solution to Eq.(36) corresponding to the cyclotron maser instability is investigated in considerable detail, treating $\beta_\perp^2\gamma_z^2/2$ as a small parameter. A careful analysis of the dispersion relation shows that the maximum growth rate is given by [Eq.(62)]

$$\omega_i = \frac{1}{2\gamma_z^2}\left[s(2\beta_\perp^2\gamma_z^4 - s)\right]^{\frac{1}{2}}\omega_{cb} ,$$

which occurs for wavenumber [Eq.(63)]

$$k = k_m = \gamma_z^2\beta_b\omega_{cb}/c.$$

Here, $s = \omega_{pb}^2/\omega_{cb}^2$ and $\gamma_z = (1-\beta_b^2)^{-\frac{1}{2}}$, and Eq.(62) includes the full influence of equilibrium self fields. The instability bandwidth Δk is also estimated in Sec. V. We obtain [Eq.(70)]

$$\frac{c(\Delta k)}{\omega_{cb}} = 2\gamma_z\left[\gamma_z^2 - \frac{1}{\beta_\perp}\left(\frac{s}{2}\right)^{\frac{1}{2}}\right]^{\frac{1}{2}} .$$

As the beam density (s) is increased, it is evident from Eq.(62) that ω_i increases to the maximum value [Eq.(64)]

$$\omega_i^{max} = \frac{1}{2}\gamma_z^2\beta_\perp^2\omega_{cb}$$

for beam density satisfying [Eq.(65)]

$$s = s_m = \beta_\perp^2\gamma_z^4 .$$

As s is increased beyond $s=s_m$, the growth rate ω_i in Eq.(62) decreases to zero for $s = s_0 = 2\beta_\perp^2\gamma_z^4$. From Eq.(70), there is a concomitant decrease in bandwidth Δk from $\Delta k = 2\gamma_z^2\omega_{cb}/c$ for $s << 2\beta_\perp^2\gamma_z^4$, to $\Delta k=0$ for $s=s_0$.

Finally, the derivation of the analytic estimates in Eqs.(62)-(65) and Eq.(70) assumes $\gamma_z^2\beta_\perp^2 << 2$. Correspondingly, $2s_m/\gamma_z^2 = 2(\omega_{pb}^2/\omega_{cb}^2)_m(1-\beta_b^2)$ $= 2\beta_\perp^2\gamma_z^2$ is assumed to be a small parameter in the derivation of the estimates in Eqs.(62)-(65) and Eq.(70). Strictly speaking, the full dispersion relation (36) should be solved numerically (Sec. IV) to determine stability properties in a regime where $2s/\gamma_z^2 \to 1$, and the equilibrium self fields are even more intense.

To summarize, depending on the value of $s = \omega_{pb}^2/\omega_{cb}^2$, the present analysis indicates that equilibrium self fields can have a large influence on the cyclotron maser instability as well as introduce a new unstable mode (the LFR branch discussed in Sec. IV). In this regard, a more precise description of self-field effects will require a stability analysis for perturbations about a <u>radially confined</u> self-consistent beam equilibrium $f_b^0(H,P_\theta,p_z)$.

II. EQUILIBRIUM CONFIGURATION AND PARTICLE TRAJECTORIES

We consider an intense relativistic electron beam propagating parallel to a uniform applied magnetic field $B_0\hat{e}_z$. The mean motion of the electron beam is in the axial and azimuthal directions, and the applied magnetic field provides radial confinement of the electrons. In equilibrium ($\partial/\partial t = 0$), the beam is assumed to be azimuthally symmetric ($\partial/\partial\theta = 0$), infinitely long, and axially uniform ($\partial/\partial z = 0$). To make the analysis tractable, we also assume that the diamagnetic self field associated with the beam rotation is negligibly small, i.e., $|B_z^s(r)| \ll B_0$. Therefore, for this equilibrium configuration, there are three single-particle constants of the motion. These are the total energy

$$H = (m^2c^4 + c^2\underset{\sim}{p}^2)^{\frac{1}{2}} - e\phi_0(r) \ , \tag{1}$$

the canonical angular momentum

$$P_\theta = rp_\theta - eB_0r^2/2c \ , \tag{2}$$

and the axial canonical momentum

$$P_z = p_z - (e/c)A_0(r) \ . \tag{3}$$

In Eqs.(1)-(3), $\underset{\sim}{p} = (p_r,p_\theta,p_z)$ is the mechanical momentum, $\phi_0(r)$ is the equilibrium electrostatic potential associated with the beam self-electric field, $A_0(r)$ is the axial component of vector potential for the equilibrium azimuthal self-magnetic field, c is the speed of light in <u>vacuo</u>, and -e and m are the electron charge and rest mass, respectively. Without loss of generality, it is assumed that the self-field potentials $\phi_0(r)$ and $A_0(r)$ are zero at r=0. For uniform beam density ($\hat{n}_b$), it will be shown later in this section that the self-field potentials in Eqs.(1) and (3)

scale as $\omega_{pb}^2 r^2/c^2$ within the electron beam ($r < r_b$). Here, $\hat{\omega}_{pb}^2 = 4\pi\hat{n}_b e^2/\gamma_b m$ is the relativistic plasma frequency-squared, and $\gamma_b mc^2$ = const. is the characteristic electron energy. Therefore, near the axis of the electron beam ($\omega_{pb}^2 r^2/c^2 \ll 1$), it follows from Eqs.(1) and (3) that

$$\begin{aligned} &p_z \ , \\ &p_\perp = (p_r^2 + p_\theta^2)^{\frac{1}{2}} \ , \end{aligned} \tag{4}$$

are approximate single-particle constants of the motion. Evidently, the approximate constants of the motion in Eq.(4) are applicable only for electron motion near the axis of the beam.

The purpose of the present analysis is to investigate the influence of self-field effects on the cyclotron maser instability in the beam interior. Therefore, we consider the class of uniform beam equilibria of the form

$$f_b^0 = f_b^0(p_\perp^2, p_z) \ . \tag{5}$$

That is, the influence of finite radial geometry is neglected in the present equilibrium and stability analysis. In addition, although the stability analysis is formulated for general choice of $f_b^0(p_\perp^2, p_z)$ in Sec. III, detailed stability properties are calculated for the specific choice of equilibrium distribution function

$$f_b^0 = \frac{\hat{n}_b}{2\pi p_\perp} \delta(p_\perp - \gamma_b m V_\perp) \, \delta(p_z - \gamma_b m V_b) \ , \tag{6}$$

where $\hat{n}_b$ = const. is the beam density, the constants V_b and $V_\perp$ are related to the relativistic mass factor γ_b by $\gamma_b = (1 - V_b^2/c^2 - V_\perp^2/c^2)^{-\frac{1}{2}}$, and the constant V_b can be identified with the average beam velocity in the axial direction. Equation (6) is a good representation of the beam distribution function in many gyrotron experiments.

As indicated earlier, we assume a uniform density ($\hat{n}_b$) nonneutral electron beam propagating parallel to the magnetic field $B_0\hat{e}_z$. It is also assumed that the current density is uniform with $J_{bz}^0(r) = -\hat{n}_b e\beta_b c$ within the beam interior. Neglecting the diamagnetic self field associated with beam rotation, the equilibrium radial self-electric and azimuthal self-magnetic fields associated with the beam space charge and axial current can be expressed as

$$\begin{aligned} \underset{\sim}{E}_0^s &= (\gamma_b m/2e)\omega_{pb}^2(x\hat{e}_x + y\hat{e}_y) \ , \\ \underset{\sim}{B}_0^s &= (\gamma_b m/2e)\omega_{pb}^2\beta_b(y\hat{e}_x - x\hat{e}_y) \ , \end{aligned} \tag{7}$$

inside the electron beam ($r \leq r_b$). Here, $\hat{e}_x$ and $\hat{e}_y$ are unit Cartesian vectors in the plane perpendicular to $B_0\hat{e}_z$, $\beta_b = V_b/c$ is the average axial velocity,

$$\omega_{pb}^2 = \frac{4\pi\hat{n}_b e^2}{\gamma_b m} \tag{8}$$

is the relativistic plasma frequency-squared,

$$\omega_{cb} = \frac{eB_0}{\gamma_b mc} \tag{9}$$

is the relativistic cyclotron frequency, and $\gamma_b mc^2 =$ const. is the characteristic electron energy. In the present analysis, it is assumed the electron energy γmc^2 is strongly peaked about $\gamma_b mc^2 =$ const., where

$$\gamma = \left(1 + \frac{p_\perp^2}{m^2c^2} + \frac{p_z^2}{m^2c^2}\right)^{\frac{1}{2}} \tag{10}$$

is the relativistic mass factor. Making use of Eq.(7), the electron trajectories [x'(t'), y'(t'), z'(t')] are determined from

$$\frac{d}{dt'} p_x' = \frac{1}{2} \gamma_b m \omega_{pb}^2 x' \left(1 - \frac{v_z'}{c} \beta_b\right) - \gamma_b m \omega_{cb} v_y' \ , \tag{11}$$

$$\frac{d}{dt'} p_y' = \frac{1}{2} \gamma_b m \omega_{pb}^2 y' \left(1 - \frac{v_z'}{c} \beta_b\right) + \gamma_b m \omega_{cb} v_x' \ , \tag{12}$$

$$\frac{d}{dt'} p_z' = \frac{1}{2} \gamma_b m \omega_{pb}^2 \beta_b c (x' v_x' + y' v_y')/c^2 \ , \tag{13}$$

within the electron beam. Here, $\underset{\sim}{v}'(t') = d\underset{\sim}{x}'(t')/dt'$ and $\underset{\sim}{p}'(t') = \gamma'(t') m \underset{\sim}{v}'(t')$. Moreover, the "initial" conditions are chosen such that $(\underset{\sim}{x}', \underset{\sim}{p}')$ passes through the phase space point $(\underset{\sim}{x}, \underset{\sim}{p})$ at time $t' = t$.

It is readily shown that Eqs.(11)-(13) possess the single-particle constants of the motion

$$\frac{d}{dt'} H' = \frac{d}{dt'} \left[\gamma' mc^2 - \frac{1}{4} \gamma_b mc^2 \frac{\omega_{pb}^2 (x'^2 + y'^2)}{c^2}\right] = 0 \ , \tag{14}$$

$$\frac{d}{dt'} P_z' = \frac{d}{dt'} \left[p_z' - \frac{1}{4} \gamma_b m \beta_b c \frac{\omega_{pb}^2 (x'^2 + y'^2)}{c^2}\right] = 0 \ , \tag{15}$$

corresponding to conservation of total energy and axial canonical momentum [Eqs.(1) and (3)]. Certain lowest-order simplifications in the particle motion are evident from Eqs.(14) and (15) for electron motion near the axis ($\omega_{pb}^2 r^2/4c^2 \ll 1$). For these electrons, it follows from Eqs.(14) and (15) that $\gamma' mc^2 \simeq$ const. and $p_z' = \gamma' m v_z' \simeq$ const. to lowest order. Therefore, expressing $p_x' = \gamma' m v_x'$ and $p_y' = \gamma' m v_y'$ with $\gamma' \simeq \gamma$ (treated as constant), and expressing $\beta_z' = v_z'/c$ with $\beta_z' \simeq \beta_z = v_z/c$

(treated as constant), the transverse orbit equations (11) and (12) reduce to

$$\frac{\gamma'}{\gamma_b}\frac{d}{dt'}v_x' = \frac{1}{2}\omega_{pb}^2 x'(1-\beta_z\beta_b) - \omega_{cb}v_y' , \tag{16}$$

$$\frac{\gamma'}{\gamma_b}\frac{d}{dt'}v_y' = \frac{1}{2}\omega_{pb}^2 y'(1-\beta_z\beta_b) + \omega_{cb}v_x' . \tag{17}$$

Equations (16) and (17) can be integrated exactly to give for the perpendicular velocity,[11]

$$v_x'(t') + iv_y'(t') = (\omega_+-\omega_-)^{-1}\Big\{[\omega_+ v_\perp \exp(i\phi) + \omega_+\omega_- r\exp(i\theta - i\pi/2)]\exp(i\omega_+\tau) - [\omega_- v_\perp \exp(i\phi) + \omega_+\omega_- r\exp(i\theta - i\pi/2)]\exp(i\omega_-\tau)\Big\} , \tag{18}$$

where $\tau = t'-t$, and ω_+ and ω_- are defined by[11]

$$\omega_\pm = \frac{\gamma_b\omega_{cb}}{2\gamma}\left\{1 \pm \left[1 - \frac{2\gamma\omega_{pb}^2}{\gamma_b^2\omega_{cb}^2}(1-\beta_z\beta_b)\right]^{\frac{1}{2}}\right\} . \tag{19}$$

For a sufficiently narrow energy spread, $\gamma \simeq \gamma_b = \text{const.}$, and the axial velocity $\beta_z = v_z/c = p_z/\gamma mc$ in Eq.(19) is approximately equal to the average value $\beta_b = \text{const.}$

In Eq.(18), the initial conditions are chosen such that $v_x'(t'=t) + iv_y'(t'=t) = v_x + iv_y \equiv v_\perp \exp(i\phi)$, and $x'(t'=t)+iy'(t'=t) = x + iy \equiv r\exp(i\theta)$. Moreover, the contribution proportional to $(2\gamma\omega_{pb}^2/\gamma_b\omega_{cb}^2)(1-\beta_z\beta_b)$ in Eq.(19) is associated with electric and magnetic self-field effects. If we take $\gamma \simeq \gamma_b$ and $\beta_z \simeq \beta_b$ in Eq.(19), it is clear that

$$(2\omega_{pb}^2/\omega_{cb}^2)(1-\beta_b^2) < 1 \tag{20}$$

is required for the equilibrium to exist and for the orbits to be radially confined. In the limit at a very tenuous electron beam with $(2\omega_{pb}^2/\omega_{cb}^2) \times (1-\beta_b^2) \ll 1$, it is clear from Eq.(19) that $\omega_+ \to \omega_c = eB_0/\gamma mc$ and $\omega_- \to 0$, and Eq.(18) reduces to the familiar result $v_x' + iv_y' = v_\perp \exp(i\phi + i\omega_c\tau)$. For finite values of $\omega_{pb}^2/\omega_{cb}^2$, however, equilibrium self-field effects modify the particle trajectories, and the perpendicular motion is <u>biharmonic</u> with oscillation components at frequencies ω_+ and ω_-. For particles sufficiently near the axis that $\omega_\pm r \ll v_\perp$, Eq.(18) is further simplified to give

$$v_x'(t') + iv_y'(t') = (\omega_+-\omega_-)^{-1}\left\{\omega_+ v_\perp \exp[i(\phi+\omega_+\tau)] - \omega_- v_\perp \exp[i(\phi+\omega_-\tau)]\right\} . \tag{21}$$

In a similar manner, we obtain

$$v_x'(t') - iv_y'(t') = (\omega_+-\omega_-)^{-1}\left\{\omega_+ v_\perp \exp[-i(\phi+\omega_+\tau)] - \omega_- v_\perp \exp[-i(\phi+\omega_-\tau)]\right\} . \tag{22}$$

III. LINEARIZED VLASOV-MAXWELL EQUATIONS

In this section, we develop the general formalism to investigate cyclotron maser stability properties for perturbations about the class of beam equilibria described by Eq.(5). For present purposes, emphasis is placed on wave perturbations interior to the electron beam. All perturbed quantities $\delta\psi(z,t)$ are expressed in the form

$$\delta\psi(z,t) = \hat{\delta\psi}\exp\{i(kz-\omega t)\} \ , \tag{23}$$

where $\mathrm{Im}\omega > 0$ corresponds to instability, and perpendicular spatial variations are assumed to be negligibly small ($\partial/\partial\underset{\sim}{x}_\perp = 0$). The transverse electromagnetic field perturbations $\delta\underset{\sim}{E} = -(1/c)\partial/\partial t(\delta\underset{\sim}{A})$ and $\delta\underset{\sim}{B} = \underset{\sim}{\nabla}\times\delta\underset{\sim}{A}$ can be expressed as

$$\begin{aligned}\delta\underset{\sim}{E} &= i(\omega/c)(\hat{\delta A}_x\hat{\underset{\sim}{e}}_x + \hat{\delta A}_y\hat{\underset{\sim}{e}}_y)\exp\{i(kz-\omega t)\} \ , \\ \delta\underset{\sim}{B} &= ik(-\hat{\delta A}_y\hat{\underset{\sim}{e}}_x + \hat{\delta A}_x\hat{\underset{\sim}{e}}_y)\exp\{i(kz-\omega t)\} \ .\end{aligned} \tag{24}$$

Moreover, the vector potential $\delta\underset{\sim}{A} = \delta A_x\hat{\underset{\sim}{e}}_x + \delta A_y\hat{\underset{\sim}{e}}_y$ is determined self-consistently in terms of the perturbed distribution function $\delta f_b(z,\underset{\sim}{p},t) = \hat{\delta f}_b(\underset{\sim}{p})\exp\{i(kz-\omega t)\}$ from the Maxwell equation

$$\left(\frac{\partial^2}{\partial z^2} - \frac{1}{c^2}\frac{\partial^2}{\partial t^2}\right)\delta\underset{\sim}{A} = \frac{4\pi e}{c}\int d^3p\,\underset{\sim}{v}\delta f_b(z,\underset{\sim}{p},t) \ . \tag{25}$$

Making use of the method of characteristics, the linearized Vlasov equation for $\delta f_b(z,\underset{\sim}{p},t)$ can be integrated to give

$$\begin{aligned}\hat{\delta f}_b(\underset{\sim}{p}) = e\int_{-\infty}^{t} dt'\exp[ik(z'-z)-i\omega(t'-t)] \\ \times\left[\hat{\delta\underset{\sim}{E}} + \frac{\underset{\sim}{v}'\times\hat{\delta\underset{\sim}{B}}}{c}\right]\cdot\frac{\partial}{\partial\underset{\sim}{p}'}\ f_b^0(p_\perp'^2,p_z') \ ,\end{aligned} \tag{26}$$

where the particle trajectories $(\underset{\sim}{x}', \underset{\sim}{p}')$ solve Eqs.(11)-(13) with "initial" conditions $\underset{\sim}{x}'(t'=t) = \underset{\sim}{x}$ and $\underset{\sim}{p}'(t'=t) = \underset{\sim}{p} = \gamma m \underset{\sim}{v}$. Substituting Eq.(24) into Eq.(26), we obtain

$$\delta\hat{f}_b(\underset{\sim}{p}) = i\frac{e}{c}\int_{-\infty}^{t} dt' \exp[ik(z'-z) - i\omega(t'-t)]$$

$$\times \left[v_x'(t')\delta\hat{A}_x + v_y'(t')\delta\hat{A}_y\right] \tag{27}$$

$$\times \left\{\frac{\gamma' m\omega}{p_\perp'}\frac{\partial}{\partial p_\perp'} + k\left(\frac{\partial}{\partial p_\perp'} - \frac{p_z'}{p_\perp'}\frac{\partial}{\partial p_\perp'}\right)\right\} f_b^0(p_\perp'^2, p_z') \ .$$

In the subsequent analysis, we define

$$\delta\hat{A}_\pm = \delta\hat{A}_x \pm i\delta\hat{A}_y \ , \tag{28}$$

where the upper sign (+) corresponds to the branch with left-hand circular polarization and the lower sign (-) corresponds to the branch with right-hand circular polarization. The combination $[v_x'\delta\hat{A}_x + v_y'\delta\hat{A}_y]$ in Eq.(27) can then be expressed as

$$\begin{aligned}&\left[v_x'(t')\delta\hat{A}_x + v_y'(t')\delta\hat{A}_y\right] \\ &= \frac{1}{2}\left[v_+'(t')\delta\hat{A}_- + v_-'(t')\delta\hat{A}_+\right] \ ,\end{aligned} \tag{29}$$

where $v_\pm'(t') = v_x'(t') \pm iv_y'(t')$ are defined in Eqs.(21) and (22) to the level of accuracy required in the present analysis.

In the curly-bracket factor $\{\cdots\}\ f_b^0(p_\perp'^2, p_z')$ in Eq.(27), we now assume that $(p_\perp', p_z')$ can be approximated by $(p_\perp, p_z)$ near the axis of the electron beam (see Sec. II). This factor is then taken outside of the t'-integral in Eq.(21). After some straightforward algebra that makes use of Eqs.(24), (25) and (27)-(29), we obtain the eigenvalue equation

$$\left(\frac{\partial^2}{\partial z^2} - \frac{1}{c^2}\frac{\partial^2}{\partial t^2}\right)\hat{\delta A}_{\pm}\exp\{i(kz-\omega t)\}$$

$$= \frac{i}{2}\frac{4\pi e^2}{c^2}\hat{\delta A}_{\pm}\exp\{i(kz-\omega t)\}$$

$$\times \int d^3p v_{\perp}\left[\frac{\gamma m\omega}{p_{\perp}}\frac{\partial f_b^0}{\partial p_{\perp}} + k\left(\frac{\partial f_b^0}{\partial p_z} - \frac{p_z}{p_{\perp}}\frac{\partial f_b^0}{\partial p_{\perp}}\right)\right] \tag{30}$$

$$\times \int_{-\infty}^{0} d\tau \exp[-i(\omega-kv_z)\tau]v'_{\pm}(t')\exp(\pm i\phi) ,$$

where $\tau = t'-t$, and $v'_{\pm}(t') = v'_x(t') \pm iv'_y(t')$ are defined in Eqs.(21) and (22). Here, $z'(t')$ has been approximated by $z'(t') = z + v_z\tau$, and use has been made of

$$\int d^3p \cdots = \int_0^{2\pi} d\phi \int_{-\infty}^{\infty} dp_z \int_0^{\infty} dp_{\perp} p_{\perp} \cdots$$

and $\int_0^{2\pi} d\phi \exp(\pm 2i\phi) = 0$ to simplify the right-hand side of Eq.(30). Note from Eq.(30) that the two equations for $\hat{\delta A}_{\pm}$ are completely decoupled. Therefore, without loss of generality, we consider the lower sign in Eq.(30) corresponding to right-circular polarization. Substituting Eq.(21) into Eq.(30) gives the dispersion relation

$$\frac{\omega^2}{c^2} - k^2 = -\frac{1}{2}\frac{4\pi e^2}{c^2}\int d^3p \frac{p_{\perp}^2}{\gamma^2 m^2}\left[\frac{\gamma m\omega}{p_{\perp}}\frac{\partial f_b^0}{\partial p_{\perp}} + k\left(\frac{\partial f_b^0}{\partial p_z} - \frac{p_z}{p_{\perp}}\frac{\partial f_b^0}{\partial p_{\perp}}\right)\right]$$

$$\times \frac{(-i)}{(\omega_+-\omega_-)}\int_{-\infty}^{0} d\tau \exp[-i(\omega-kv_z)\tau][\omega_+\exp(i\omega_+\tau) \tag{31}$$

$$- \omega_-\exp(i\omega_-\tau)] .$$

Introducing the re-normalized distribution function $F_b(p_{\perp}^2, p_z)$ defined by

$$f_b^0(p_\perp^2,p_z) = \frac{\hat{n}_b}{2\pi} F_b(p_\perp^2,p_z) \ , \tag{32}$$

and carrying out the time integration in Eq.(31), the dispersion relation can be expressed as

$$\frac{\omega^2}{c^2} - k^2 = - \frac{2\pi\hat{n}_b e^2}{c^2} \int_0^\infty dp_\perp \int_{-\infty}^\infty dp_z \frac{p_\perp^2}{\gamma^2 m^2} I \left[(\gamma m\omega - kp_z) \frac{\partial F_b}{\partial p_\perp} + kp_\perp \frac{\partial F_b}{\partial p_z} \right] \ , \tag{33}$$

where the orbit integral I is defined by

$$I = \frac{\gamma(\gamma\omega - kp_z/m)}{(\gamma\omega - kp_z/m)^2 - \omega_{c0}(\gamma\omega - kp_z/m) + \omega_{p0}^2(\gamma - \beta_b p_z/mc)/2} \ . \tag{34}$$

In Eq.(34), $\omega_{c0} = eB_0/mc$ is the nonrelativistic cyclotron frequency, and $\omega_{p0}^2 = 4\pi e^2\hat{n}_b/m$ is the nonrelativistic plasma frequency-squared. In obtaining Eq.(34), use has been made of the definition of $\omega_\pm$ in Eq.(19).

For present purposes, we specialize to the choice of distribution function in Eq.(6), which corresponds to

$$F_b(p_\perp^2,p_z) = \frac{1}{p_\perp} \delta(p_\perp - \gamma_b m V_\perp)\delta(p_z - \gamma_b m\beta_b c) \ . \tag{35}$$

Here, the relativistic mass factor γ_b is defined by $\gamma_b = (1 - V_b^2/c^2 - V_\perp^2/c^2)^{-\frac{1}{2}}$ where $V_b = \beta_b c$ is the average velocity in the axial direction. After some tedious but straightforward algebra that makes use of Eqs.(34) and (35), the dispersion relation (33) can be expressed as

$$\begin{aligned} \frac{\omega^2}{c^2} - k^2 = {} & \frac{\omega_{pb}^2}{c^2} \frac{(\omega - k\beta_b c)^2}{(\omega - k\beta_b c)^2 - \omega_{cb}(\omega - k\beta_b c) + \omega_{pb}^2(1-\beta_b^2)/2} \\ & - \frac{\omega_{pb}^2}{2c^2} \beta_\perp^2 \frac{(\omega^2 - k^2c^2)[(\omega - k\beta_b c)^2 - (\omega_{pb}^2/2)(1-\beta_b^2)] + (\omega - k\beta_b c)^2(\omega_{pb}^2/2)}{[(\omega - k\beta_b c)^2 - \omega_{cb}(\omega - k\beta_b c) + (\omega_{pb}^2/2)(1-\beta_b^2)]^2} \ , \end{aligned} \tag{36}$$

where $\beta_\perp = V_\perp/c$, $\omega_{cb} = eB_0/\gamma_b mc$, and $\omega_{pb}^2 = 4\pi\hat{n}_b e^2/\gamma_b/m$. Introducing the frequencies $\omega_b^\pm$ defined by

$$\omega_b^\pm = \frac{1}{2}\,\omega_{cb}\left\{1 \pm [1 - (2\omega_{pb}^2/\omega_{cb}^2)(1-\beta_b^2)]^{\frac{1}{2}}\right\} \quad , \tag{37}$$

the dispersion relation (36) can be expressed in the equivalent form

$$\frac{\omega^2}{c^2} - k^2 = \frac{\omega_{pb}^2}{c^2}\,\frac{(\omega-k\beta_b c)^2}{(\omega-k\beta_b c-\omega_b^+)(\omega-k\beta_b c-\omega_b^-)}$$

$$- \frac{\omega_{pb}^2}{2c^2}\,\beta_\perp^2\,\frac{(\omega^2-k^2c^2)[(\omega-k\beta_b c)^2 - (\omega_{pb}^2/2)(1-\beta_b^2)] + (\omega-k\beta_b c)^2(\omega_{pb}^2/2)}{(\omega-k\beta_b c-\omega_b^+)^2(\omega-k\beta_b c-\omega_b^-)^2} \quad . \tag{38}$$

Note from Eqs.(19) and (37) that $\omega_b^\pm \equiv \omega_\pm(\gamma=\gamma_b,\ \beta_z=\beta_b)$.

Equation (36) [or Eq.(38)] consititutes one of the main results of this paper and can be used to investigate stability properties for a broad range of system parameters. In this regard, we emphasize that Eq.(36) has been derived with no a priori assumption that $\beta_\perp^2 << 1$ or that $\beta_b^2 << 1$.

IV. ANALYSIS OF THE DISPERSION RELATION

We now investigate the stability properties predicted by Eq.(36). In the limit of a tenuous electron beam with $(2\omega_{pb}^2/\omega_{cb}^2)(1-\beta_b^2) \ll 1$, the self fields are negligibly small and $\omega_b^+ \to \omega_{cb}$ and $\omega_b^- \to 0$ in Eq.(37). The corresponding dispersion relation (36) [or Eq.(38)] for the cyclotron maser instability in the tenuous beam limit reduces to the familiar result[12,13]

$$\frac{\omega^2}{c^2} - k^2 = \frac{\omega_{pb}^2}{c^2}\,\frac{(\omega-k\beta_b c)}{\omega-k\beta_b c-\omega_{cb}} - \frac{\omega_{pb}^2}{2c^2}\,\beta_\perp^2\,\frac{\omega^2-k^2c^2}{(\omega-k\beta_b c-\omega_{cb})^2}\,. \tag{39}$$

Note that Eq.(39) exhibits resonant behavior when the cyclotron resonance condition

$$\omega-k\beta_b c = \omega_{cb} \tag{40}$$

is satisfied. We refer to Eq.(39), valid for $(2\omega_{pb}^2/\omega_{cb}^2)(1-\beta_b^2) \ll 1$, as the reference dispersion relation (RDR).

On the other hand, for finite, non-zero values of $(2\omega_{pb}^2/\omega_{cb}^2)(1-\beta_b^2)$, it is clear from Eq.(38) that there are two resonance conditions. These are:

$$\omega-k\beta_b c = \omega_b^+ = \frac{\omega_{cb}}{2}\left\{1 + \left[1 - \frac{2\omega_{pb}^2}{\omega_{cb}^2}\,(1-\beta_b^2)\right]^{\frac{1}{2}}\right\}, \tag{41}$$

and

$$\omega-k\beta_b c = \omega_b^- = \frac{\omega_{cb}}{2}\left\{1 - \left[1 - \frac{2\omega_{pb}^2}{\omega_{cb}^2}\,(1-\beta_b^2)\right]^{\frac{1}{2}}\right\}. \tag{42}$$

The resonance condition in Eq.(41) represents a generalization of the cyclotron resonance condition in Eq.(40) to include the influence of equilibrium self-field effects. The resonance condition in Eq.(42), which also occurs in calculations of the spontaneous emission from a test electron,[10] is entirely associated with self-field effects. It should also be pointed out that the term proportional to $\beta_\perp^2$ on the right-hand side of Eq.(38) drives the instability, whereas the first term [the term proportional to $(\omega-k\beta_b c)^2$] on the right-hand side of Eq.(38) has a stabilizing influence.

For the case of relatively low beam density satisfying

$$s = \omega_{pb}^2/\omega_{cb}^2 << 1 \ , \tag{43}$$

Eq.(38) can be approximated by

$$\frac{\omega^2}{c^2} - k^2 = \frac{\omega_{pb}^2\omega_b^+}{c^2(\omega_b^+-\omega_b^-)}\,\frac{(\omega-k\beta_b c)}{(\omega-k\beta_b c-\omega_b^+)} - \frac{\omega_{pb}^2}{2c^2}\beta_\perp^2\,\frac{(\omega^2-k^2c^2)[(\omega_b^+)^2 - (\omega_{pb}^2/2)(1-\beta_b^2)] + (\omega_b^+)^2(\omega_{pb}^2/2)}{(\omega_b^+-\omega_b^-)^2(\omega-k\beta_b c-\omega_b^+)^2} \tag{44}$$

for the <u>high frequency resonance</u> (HFR) $\omega-k\beta_b c\simeq\omega_b^+$, and by

$$\frac{\omega^2}{c^2} - k^2 = -\frac{\omega_{pb}^2\omega_b^-}{c^2(\omega_b^+-\omega_b^-)}\,\frac{(\omega-k\beta_b c)}{(\omega-k\beta_b c-\omega_b^-)} - \frac{\omega_{pb}^2}{2c^2}\beta_\perp^2\,\frac{(\omega^2-k^2c^2)[(\omega_b^-)^2 - (\omega_{pb}^2/2)(1-\beta_b^2)] + (\omega_b^-)^2(\omega_{pb}^2/2)}{(\omega_b^+-\omega_b^-)^2(\omega-k\beta_b c-\omega_b^-)^2} \tag{45}$$

for the <u>low frequency resonance</u> (LFR) $\omega-k\beta_b c\simeq\omega_b^-$. Note that the final term in Eq.(45) is proportional to $(\omega_b^-)^2$, which vanishes in the limit of

negligibly small self fields with $(2\omega_{pb}^2/\omega_{cb}^2)(1-\beta_b^2) \to 0$. Thus, for relatively low beam density satisfying Eq.(43), the dominant stability behavior is governed by the approximate dispersion relation in Eq.(44).

The growth rate $\omega_i = Im\omega$ and real oscillation frequency $\omega_r = Re\omega$ have been calculated numerically from the complete dispersion relation in Eq.(36) [or Eq.(38)] for a broad range of system parameters, $\beta_\perp$, β_b, $s \equiv \omega_{pb}^2/\omega_{cb}^2$, and kc. Because most gyrotron experiments operate at relatively small axial wavenumber satisfying $k^2c^2/\omega_{cb}^2 < 1$, in the present analysis the allowable range of the wavenumber k is restricted to $-\omega_{cb} < kc < \omega_{cb}$. Shown in Fig. 1 are plots of (a) the normalized Doppler-shifted real frequency $(\omega_r - k\beta_b c)/\omega_{cb}$, and (b) the normalized growth rate ω_i/ω_{cb} versus kc/ω_{cb} obtained from Eq.(36) for $\beta_\perp = 0.5$, $\beta_b = 0.2$ and $s = 0.05$. In Fig. 1(a), the solid curves correspond to stable oscillations with $Im\omega = 0$, and the broken curves correspond to the real frequency of the unstable solutions to Eq.(36) with $Im\omega = \omega_i > 0$. For each real value of kc, Eq.(36) supports six solutions for ω, with the complex roots occurring in conjugate pairs. Several features are noteworthy from Fig. 1. First, the unstable solution with Doppler-shifted real frequency close to ω_{cb} in Fig. 1(a) corresponds to to the high frequency resonance (HFR) defined in Eq.(41). The unstable solution with small Doppler-shifted real frequency in Fig. 1(a) corresponds to the low frequency resonance (LFR) defined in Eq.(42). This general feature (two classes of unstable modes) persists over the entire range of system parameters s, $\beta_\perp$ and β_b. Second, for small positive values of wavenumber satisfying $kc/\omega_{cb} \gtrsim 0$, the LFR branch in Fig. 1 exhibits two unstable solutions. In this regard, the unstable LFR mode with $\omega_r - k\beta_b c > 0$ in Fig. 1(a) originates from the interaction between the two modes $\omega=kc$ and $\omega=k\beta_b c+\omega_b^-$. This interaction is expected and the instability persists as the beam density (as measured by the self-field parameter s) is increased.

On the other hand, the unstable LFR mode with $\omega_r - k\beta_b c < 0$ in Fig. 1(a) originates from the interaction between the two modes $\omega = -kc$ and $\omega = k\beta_b c + \omega_b^-$. this is a weak interaction and the instability occurs only over a limited range of s and β_b. As evident from Fig. 1(b), the growth rate of this particular LFR mode is small. Therefore, this mode is neglected in the subsequent analysis. Third, as evident from Fig. 1(b), even at moderately low beam density (s = 0.05), the maximum growth rate of the low frequency resonance mode can be a substantial fraction of that of the high frequency resonance mode.

Introducing the wave phase velocity V_p defined by $V_p = \omega_r/k$ we identify "fast" and "slow" waves by $V_p^2 > c^2$ and $V_p^2 < c^2$, respectively. A careful examination of Fig. 1(a) shows that a portion of the HFR branch corresponds to fast-wave propagation and a portion corresponds to slow-wave propagation. For example, in Fig. 1(a), the region $kc/\omega_{cb} < -0.9$ ($kc/\omega_{cb} > -0.7$) corresponds to slow-wave (fast-wave) propagation for the HFR branch. Because gyrotron experiments typically operate in a waveguide or cavity, only the fast-wave solution corresponds to a propagating electromagnetic mode where the azimuthal bunching mechanism dominates. On the other hand, the slow-wave solution, with phase velocity smaller than the speed of light, is a non-propagating mode in a waveguide, at least in the limit of a tenuous electron beam. In addition, the instability mechanism for the slow-wave solution is axial electron bunching in the direction of wave propagation. We also find from Fig. 1(a) that most of the low frequency resonance branch corresponds to slow-wave propagation. Moreover, the fast-wave portion of the high frequency resonance branch in Fig. 1 can be identified with the conventional cyclotron maser instability, modified by equilibrium self-field effects. In practical circumstances, the slow-wave portion of the low frequency resonance branch may deteriorate the beam quality in high-current gyrotron operation.

As a reference calculation, in Fig. 2 we present solutions of the reference dispersion relation (RDR) in Eq.(39), valid in the limit of negligibly small self fields with $(2\omega_{pb}^2/\omega_{cb}^2)(1-\beta_b^2) \to 0$. In particular, Fig. 2 shows plots versus kc/ω_{cb} of (a) the Doppler-shifted real frequency $(\omega_r - k\beta_b c)/\omega_{cb}$, and (b) the growth rate ω_i/ω_c obtained from Eq.(39) for $\beta_\perp = 0.5$, $\beta_b = 0.2$ and $s = 0.05$. Comparing Fig. 2(a) with Fig. 1(a), it is evident that the low frequency resonance mode is absent in the reference dispersion relation (39). Moreover, for the low beam density ($s = 0.05$) assumed in Figs. 1 and 2, the real frequency and growth rate of the high frequency resonance mode calculated from Eq.(39) are almost identical to those calculated from the full dispersion relation in Eq.(36). At higher beam densities, however, the stability properties calculated from Eqs.(36) and (39) can differ substantially.

Of considerable practical interest are the growth rate and real oscillation frequency of the high frequency resonance (HFR) mode as the self field parameter $s = \omega_{pb}^2/\omega_{cb}^2$ is increased. Typical results obtained from Eq.(36) [or Eq.(38)] are shown in Fig. 3, where (a) the Doppler-shifted real frequency $(\omega_r - k\beta_b c)/\omega_{cb}$, and (b) the growth rate ω_i/ω_{cb} are plotted versus kc/ω_{cb} for $\beta_\perp = 0.5$, $\beta_b = 0.2$ and several values of s ranging from 0.1 to 0.5. In Fig. 3, the solid and dashed curves represent the fast- and slow-wave solutions, respectively, for the HFR branch. Remarkably, the Doppler-shifted real frequency $(\omega_r - k\beta_b c)$ of the fast-wave solution (corresponding to the cyclotron maser instability) is approximately equal to ω_{cb} over the entire range of wavenumber k corresponding to instability ($\omega_i > 0$). Equally remarkable, the real oscillation frequency of the cyclotron maser instability satisfies $\omega_r - k\beta_b c \simeq \omega_{cb}$ for beam densities ranging from $s = 0.1$ to $s = 0.5$ [Fig. 3(a)]. For $\beta_\perp = 0.5$ and $\beta_b = 0.2$, we also note from Fig. 3(b) that the maximum growth rate of the cyclotron maser

instability increases as the beam density is increased from s = 0.1 to s = 0.3, and then decreases for s = 0.4 and s = 0.5.

In order to complete the numerical analysis of the dispersion relation (36), we now present stability results for the low frequency resonance (LFR) mode for s ranging from 0.1 to 0.5. Shown in Fig. 4 are plots versus kc/ω_{cb} of (a) the Doppler-shifted real frequency $(\omega_r - k\beta_b c)/\omega_{cb}$, and (b) the growth rate ω_i/ω_{cb} obtained from Eq.(36) for the low frequency resonance mode for $\beta_\perp = 0.5$, $\beta_b = 0.2$ and several values of s. In Fig. 4, the solid and dashed portions of the curves represent the fast- and slow-wave solutions, respectively. Although the growth rate of the low frequency resonance mode is substantial for the values of beam density assumed in Fig. 4, the real oscillation frequency is much less than that of the cyclotron maser instability considered in Fig. 3. In addition, most of the low frequency resonance mode with sizeable growth rate corresponds to the slow-wave solution. That portion of the low frequency resonance mode corresponding to the fast-wave solution does have substantial growth rate at moderate beam density. This fast-wave solution may be a plausible candidate for microwave generation, in addition to the cyclotron maser instability (appropriately modified by self-field effects).

V. CYCLOTRON MASER INSTABILITY

In Sec. IV, we identified the cyclotron maser instability appropriately modified by self-field effects as the fast-wave portion of the high frequency resonance branch in Eq.(36) [or Eq.(38)]. Because present-day gyrotron experiments operate in a regime corresponding to the cyclotron maser instability, in this section we make use of Eq.(36) to investigate detailed properties of the cyclotron maser instability including the important influence of self-field effects. For notational convenience in the subsequent analysis, we introduce the frequency ω' and axial wavenumber k' in a frame of reference moving with the axial velocity $\beta_b c$ of the electron beam. The frequency ω and wavenumber k in the laboratory frame are related to ω' and k' by

$$\omega = \gamma_z(\omega' + k'\beta_b c) \ , \tag{46}$$

and

$$k = \gamma_z(k' + \omega'\beta_b/c) \ , \tag{47}$$

where $\gamma_z \equiv (1-\beta_b^2)^{-\frac{1}{2}}$ is the relativistic mass factor associated with the axial motion. Substituting Eqs.(46) and (47) into Eq.(36), it is straightforward to show that the dispersion relation in the beam frame is given by

$$\frac{\omega'^2}{c^2} - k'^2 = \frac{\omega_{pb}^2}{c^2}\frac{\omega'^2}{\omega'^2 - \omega_{cb}\gamma_z\omega' + \omega_{pb}^2/2} - \frac{\omega_{pb}^2}{2c^2}\beta_\perp^2\gamma_z^2\frac{(\omega'^2-k'^2c^2)(\omega'^2-\omega_{pb}^2/2) + \omega'^2\omega_{pb}^2/2}{(\omega'^2 - \omega_{cb}\gamma_z\omega' + \omega_{pb}^2/2)^2} \ . \tag{48}$$

As evident from Fig. 3(a) in Sec. IV, the real oscillation frequency ω_r' of the cyclotron maser instability is approximately equal to $\gamma_z\omega_{cb}$

over a wide range of system parameters $\beta_\perp$, β_b and $s = \omega_{pb}^2/\omega_{cb}^2$. That is,

$$\omega' \simeq \gamma_z \omega_{cb} \tag{49}$$

is an excellent approximation for the range of system parameters investigated in Sec. IV. A more detailed analysis (later in Sec. V) shows that Eq.(49) is generally valid provided

$$\frac{1}{2}\gamma_z^2\beta_\perp^2 << 1 \quad . \tag{50}$$

The inequality in Eq.(50) is easily satisfied in the parameter range of present-day gyrotron experiments. We now introduce the normalized wavenumber ζ and eigenfrequency Z defined by

$$\zeta = k'c/\omega_{cb} \ , \tag{51}$$

and

$$\begin{aligned} Z &= \frac{(\omega' - \gamma_z\omega_{cb})\gamma_z}{\omega_{cb}} + \frac{1}{2}s \\ &= \frac{(\omega - k\beta_b c - \omega_{cb})\gamma_z^2}{\omega_{cb}} + \frac{1}{2}s. \end{aligned} \tag{52}$$

Making use of Eqs.(49), (51) and (52), it is straightforward to show that the dispersion relation in Eq.(48) can be approximated by

$$\begin{aligned} &(\gamma_z^2 - \zeta^2)Z^2 - s\gamma_z^2 Z \\ &+ \frac{1}{2}\beta_\perp^2\gamma_z^2 s[\gamma_z^4 - \zeta^2(\gamma_z^2 - \tfrac{1}{2}s)] = 0 \ , \end{aligned} \tag{53}$$

where $s = \omega_{pb}^2/\omega_{cb}^2$ is defined in Eq.(43). Equation (53) is a quadratic equation for Z and can be readily solved.

Introducing the function $h(\zeta^2,s)$ defined by

$$h^2(\zeta^2,s) = \frac{1}{2} s\beta_\perp^2\gamma_z^2 \frac{\gamma_z^4-\zeta^2(\gamma_z^2 - s/2)}{\gamma_z^2 - \zeta^2} - \frac{1}{4} \frac{s^2\gamma_z^4}{(\gamma_z^2 - \zeta^2)^2} , \tag{54}$$

the necessary and sufficient condition for Eq.(53) to exhibit instability ($Im\omega' > 0$) is given by

$$h^2(\zeta^2,s) > 0 . \tag{55}$$

In addition, when Eq.(55) is satisfied, the normalized growth rate $Z_i = ImZ = Im\omega'/\omega_{cb}$ for the unstable branch can be expressed as

$$Z_i = h(\zeta^2,s) \tag{56}$$

for specified wavenumber (ζ) and beam density (s). A careful analysis of the function $h^2(\zeta^2,s)$ defined in Eq.(54) shows the following properties.

(a) The values of $h^2(\zeta^2,s)$ at $\zeta^2 = -\infty$ and $\zeta^2=0$ are given by

$$h^2(-\infty,s) = h_\infty^2 = \frac{1}{4} s\gamma_z^2\beta_\perp^2(2\gamma_z^2-s) , \tag{57}$$

and

$$h^2(0,s) = h_0^2 = \frac{1}{4} s(2\beta_\perp^2\gamma_z^4-s) . \tag{58}$$

(b) The function $h^2(\zeta^2,s)$ assumes its maximum value

$$h^2(\zeta_m^2,s) = h_m^2 = \frac{1}{4} s\beta_\perp^2\gamma_z^2(2\gamma_z^2-s) + \frac{1}{16} s^2\beta_\perp^4\gamma_z^4 \tag{59}$$

at

$$\zeta^2 = \zeta_m^2 \equiv -(2/\beta_\perp^2)(1 - \gamma_z^2\beta_\perp^2/2) \ . \tag{60}$$

(c) For specified values of s, γ_z and $\beta_\perp$, the function $h^2(\zeta^2,s)$ vanishes for normalized wavenumber satisfying

$$\zeta^2 = \zeta_0^2 = \frac{\gamma_z^2(2\gamma_z^2 - s/2)}{2(\gamma_z^2 - s/2)} \times \left\{ 1 - \left[1 - \frac{2(\gamma_z^2 - s/2)(2\gamma_z^4\beta_\perp^2 - s)}{\beta_\perp^2\gamma_z^2(2\gamma_z^2 - s/2)^2} \right]^{\frac{1}{2}} \right\} . \tag{61}$$

(d) Finally, we note from Eq.(54) that $h^2(\zeta^2,s)$ exhibits singular behavior at $\zeta^2 = \gamma_z^2$.

Shown in Fig. 5 is a schematic plot of $h^2(\zeta^2,s)$ versus ζ^2 assuming $\gamma_z^2\beta_\perp^2 < 2$, which is consistent with Eq.(50). In Fig. 5, only the region $\zeta^2 \geq 0$ is physically acceptable. Moreover, the region $\zeta^2 > \gamma_z^2$ corresponds to slow-wave solutions, which are excluded in the subsequent stability analysis.

In the region $0 \leq \zeta^2 < \gamma_z^2$ corresponding to the cyclotron maser instability, the function $h^2(\zeta^2,s)$ assumes its maximum value $h^2(0,s) = h_0^2$ at $\zeta^2 = 0$. Therefore, making use of Eqs.(47), (49), (51), (52), and (58), it can be shown that the maximum growth rate of the cyclotron maser instability is given by

$$\omega_i = \frac{1}{2\gamma_z^2}[s(2\beta_\perp^2\gamma_z^4 - s)]^{\frac{1}{2}}\omega_{cb} \ , \tag{62}$$

which occurs for axial wavenumber

$$k = k_m = \gamma_z^2\beta_b\omega_{cb}/c \tag{63}$$

in the laboratory frame. As a function of s, the maximum growth rate in Eq.(62) increases with increasing beam density (s), and achieves the maximum value

$$\omega_i^{max} = \frac{1}{2}\gamma_z^2\beta_\perp^2\omega_{cb} , \tag{64}$$

for beam density satisfying

$$s = s_m = \beta_\perp^2\gamma_z^4 . \tag{65}$$

For $s > s_m = \beta_\perp^2\gamma_z^4$, the maximum growth rate in Eq.(62) decreases to zero as s approaches $s_0 = 2\beta_\perp^2\gamma_z^4$.

Shown in Fig. 6 are plots of the maximum normalized growth rate ω_i/ω_{cb} versus the parameter s for $\zeta=0$, $\beta_\perp=0.5$ and $\beta_b=0.2$. The dashed, solid, and dotted curves are obtained from Eqs.(62), (36) and (39) respectively. The two curves obtained from Eqs.(36) and (62) are almost identical. We therefore conclude that Eq (62) is an excellent estimate of the maximum growth rate of the cyclotron maser instability. It is evident from the dotted curve in Fig. 6 that the reference dispersion relation (39), which neglects self-field effects, gives an increasingly poor estimate of the maximum growth rate for $s \gtrsim 0.2$.

As indicated earlier, gyrotron experiments are typically carried out in a waveguide. To maximize the growth rate and efficiency of microwave generation, it is required that the group velocity of the vacuum waveguide mode be approximately equal to the beam velocity, i.e.,

$$V_g = \frac{d\omega}{dk} = \frac{kc^2}{\omega} \simeq \beta_b c . \tag{66}$$

The condition for cyclotron resonance is

$$\omega \simeq k\beta_b c + \omega_{cb} . \tag{67}$$

Solving Eqs.(66) and (67) simultaneously gives $k = k_m = \gamma_z^2 \beta_b \omega_{cb}/c$, which is identical to Eq.(63). This is an alternate way to estimate the wavenumber $k = k_m$ corresponding to maximum growth.

The condition for existence of the equilibrium in Eq.(20) can be expressed in the equivalent form

$$s < \frac{\gamma_z^2}{2} . \tag{68}$$

In circumstances where γ_z^2 exceeds 2s by a sufficiently large amount, the quantity ζ_0^2 defined in Eq.(61) can be approximated by

$$\zeta_0^2 = \gamma_z^2 - \frac{1}{\beta_\perp}\left(\frac{s}{2}\right)^{\frac{1}{2}} . \tag{69}$$

From Fig. 5 and Eq.(56), we conclude that the cyclotron maser instability exists only for ζ in the range $-\zeta_0 < \zeta < \zeta_0$. Of considerable practical interest is the bandwidth of the instability. In this regard, we define the effective wavenumber bandwidth Δk by

$$\Delta k = 2\gamma_z \zeta_0 \omega_{cb}/c$$

$$= 2\gamma_z\left[\gamma_z^2 - \frac{1}{\beta_\perp}\left(\frac{s}{2}\right)^{\frac{1}{2}}\right]^{\frac{1}{2}} \frac{\omega_{cb}}{c} , \tag{70}$$

which represents the range in k-space for which instability exists ($\omega_i > 0$). Shown in Fig. 7 are plots of the normalized bandwidth $c(\Delta k)/\omega_{cb}$ versus the parameter s for $\beta_\perp = 0.5$ and $\beta_b = 0.2$. The solid, dashed, and dotted curves correspond to the bandwidths calculated from Eqs.(36), (70) and (39), respectively. Evidently, the analytic estimate of Δk in Eq.(70) gives good agreement with the bandwidth calculated from the full dispersion

relation in Eq.(36). On the other hand, the reference dispersion relation (39), which neglects equilibrium self-field effects, gives an overestimate of the bandwidth which becomes increasingly poor at larger values of s. Note from Fig. 7 [and from Fig. 3(b)] that the bandwidth Δk of the cyclotron maser instability decreases as s increases.

Finally, we make use of Eq.(53) to estimate the real frequency shift $\delta\omega_r = \Delta(\omega_r - k\beta_b c - \omega_{cb})$ from exact cyclotron resonance ($\omega_r - k\beta_b c - \omega_{cb} = 0$). The frequency shift $\delta\omega_r$ is directly associated with the efficiency of radiation generation. From Eq.(53), it is readily shown that

$$Z_r = \mathrm{Re}Z = \frac{1}{2}\,\frac{s\gamma_z^2}{\gamma_z^2 - \zeta^2} \tag{71}$$

in the unstable region of parameter space [$h^2(\zeta^2,s) > 0$ in Eq.(55)]. Making use of the definition of Z in Eq.(52), the frequency shift $\delta\omega_r$ can be expressed as

$$\delta\omega_r = \Delta(\omega_r - k\beta_b c - \omega_{cb}) = \frac{s\omega_{cb}}{2\gamma_z^2}\,\frac{\zeta^2}{\gamma_z^2 - \zeta^2}\,. \tag{72}$$

From Eq.(72), we note that the frequency shift $\delta\omega_r$ increases from zero as the parameter ζ^2 increases. Shown in Fig. 8 are plots of the normalized frequency shift $\delta\omega_r/\omega_{cb}$ versus s for $\beta_\perp = 0.5$, $\beta_b = 0.2$, and $\zeta = 0$ corresponding to the maximum growth rate. The solid and dotted curves are calculated from Eqs.(34) and (39), respectively. The analytic estimate of $\delta\omega_r$ in Eq.(72) predicts zero frequency shift (i.e., $\delta\omega_r = 0$) for $\zeta = 0$. Given the sizeable deviation of $\delta\omega_r$ from zero calculated from Eq.(36) for $s > 0.1$, it is clear from Fig. 8 that the analytic estimate of $\delta\omega_r$ in Eq.(72) fails at moderate beam density. Moreover, the reference dispersion relation (39), which neglects equilibrium self-field effects, gives an even

larger error (as well as the incorrect sign) in estimating the frequency shift $\delta\omega_r$ (compare the dotted and solid curves in Fig. 8).

The maximum frequency shift calculated from Eq.(72) is given by

$$\delta\omega_r = \left(\frac{s}{2}\right)^{\frac{1}{2}}\left[\beta_\perp - \frac{1}{\gamma_z^2}\left(\frac{s}{2}\right)^{\frac{1}{2}}\right]\omega_{cb} , \tag{73}$$

which occurs for $\zeta^2 = \zeta_0^2$, corresponding to the stability boundary $h(\zeta_0^2,s) = 0$ in Fig. 5. In obtaining Eq.(73), use has been made of Eq.(69) and (72). The frequency shift $\delta\omega_r$ in Eq.(73) assumes the maximum value

$$\delta\omega_r^{max} = \frac{1}{4}\gamma_z^2\beta_\perp^2\omega_{cb} , \tag{74}$$

which occurs at the beam density

$$s = \frac{1}{2}\gamma_z^4\beta_\perp^2 . \tag{75}$$

Provided $\gamma_z^2\beta_\perp^2 \ll 1$ [see also Eq.(50)], we note from Eqs.(64) and (74) that both the real frequency shift $\delta\omega_r$ and the growth rate ω_i are sufficiently small that the approximation in Eq.(49) is valid. Moreover, because the estimate of ζ_0^2 in Eq.(69) has assumed $2s \ll \gamma_z^2$, it should be reiterated that the expression for the wavenumber bandwidth Δk in Eq.(73) breaks down for sufficiently high beam density that $s \to \gamma_z^2/2$.

VI. CONCLUSIONS

In the present analysis, we have made use of the Vlasov-Maxwell equations to investigate detailed properties of the cyclotron maser instability including the important influence of intense equilibrium self fields. Following a discussion of the equilibrium configuration and particle trajectories (Sec. II), the general stability formalism was developed (Sec. III) for body-wave perturbations localized near the axis (r=0) of the electron beam. The resulting dispersion relation in Eq.(36) [or Eq.(38)] includes the influence of intense equilibrium self fields on stability behavior. In Eq.(36), two distinct types of resonance were identified, namely, the high frequency resonance ($\omega - k\beta_b c \simeq \omega_b^+$), and the low frequency resonance ($\omega - k\beta_b c \simeq \omega_b^-$). In Sec. IV, the dispersion relation (36) was solved numerically over a wide range of system parameters. While the majority of the low frequency resonance (LFR) branch corresponds to a slow-wave solution, it was found that the high frequency resonance (HFR) branch corresponds primarily to a fast-wave solution with $\omega_r - k\beta_b c \simeq \omega_{cb}$ over a wide range of system parameters. This mode was identified with the cyclotron maser instability, appropriately modified by equilibrium self-field effects.

In Sec. V, the mode corresponding to the cyclotron maser instability was investigated in considerable detail. After a careful analysis of the dispersion relation, treating $\beta_\perp^2\gamma_z^2/2$ as a small parameter, it was shown that the maximum growth rate is [Eq.(62)]

$$\omega_i = \frac{1}{2\gamma_z^2}[s(2\beta_\perp^2\gamma_z^4 - s)]^{\frac{1}{2}}\omega_{cb} ,$$

which occurs for wavenumber $k = k_m = \gamma_z^2\beta_b\omega_{cb}/c$. Here, $s = \omega_{pb}^2/\omega_{cb}^2$, and the influence of intense equilibrium self fields is fully incorporated

in Eq. (62). In Sec. V, the instability bandwidth Δk was estimated to be [Eq.(70)]

$$\frac{c(\Delta k)}{\omega_{cb}} = 2\gamma_z \left[\gamma_z^2 - \frac{1}{\beta_\perp}\left(\frac{s}{2}\right)^{\frac{1}{2}}\right]^{\frac{1}{2}} .$$

Evidently, the bandwidth Δk decreases monotonically to zero as the self-field parameter s approaches $s_0 = 2\beta_\perp^2\gamma_z^4$. Moreover, from Eq.(62), maximum growth occurs for $s = s_m = \beta_\perp^2\gamma_z^4$.

To summarize, depending on the value of $s = \omega_{pb}^2/\omega_{cb}^2$, the present analysis indicates that equilibrium self fields can have a large influence on the cyclotron maser instability as well as introduce a new unstable mode (the LFR branch discussed in Sec. IV). In this regard, a more precise description of self-field effects will require a stability analysis for perturbations about a radially-confined self-consistent beam equilibrium $f_b^0(H,P_\theta,p_z)$.

ACKNOWLEDGMENTS

This research was supported by the Office of Naval Research.

VII. REFERENCES

1. V.A. Flyagin, A.V. Gaponov, M.I. Petelin, and V.K. Yulpatov, IEEE Trans. Microwave Theory Tech. MTT-25, 514 (1977).
2. J.L. Hirschfield and V.L. Granatstein, IEEE Trans. Microwave Theory Tech. MTT-25, 528 (1977).
3. K.E. Kreischer, J.B. Schutkeker, B.G. Danly, W.J. Mulligan and R.J. Temkin, Int. J. Electronics 57, 835 (1984), and references therein.
4. H.S. Uhm, R.C. Davidson and K.R. Chu, Phys. Fluids 21, 1877 (1978).
5. K.R. Chu, Phys. Fluids 21, 2354 (1978), and references therein.
6. H.S. Uhm and R.C. Davidson, Phys. Fluids 23, 2538 (1980).
7. H.S. Uhm, J.Y. Choe and S. Ahn, Int. J. Electronics 51, 521 (1981).
8. H.S. Uhm and J.Y. Choe, J. Appl. Phys. 53, 8483 (1982).
9. H.S. Uhm and J.Y. Choe, Phys. Fluids 26, 3418 (1983).
10. R.C. Davidson and W.A. McMullin, Phys. Fluids 27, 1268 (1984).
11. R.C. Davidson, in Handbook of Plasma Physics - Volume 2: Basic Plasma Physics (Eds. M.N. Rosenbluth and R.Z. Sagdeev, Elsevier Science Publishers, 1984) pp. 731-819.
12. R.C. Davidson and W.A. McMullin, Phys. Fluids, 26, 840 (1983).
13. K.R. Chu and J.L. Hirschfield, Phys. Fluids 21, 461 (1978).

FIGURE CAPTIONS

Fig. 1. Plots of (a) the normalized Doppler-shifted real frequency $(\omega_r - k\beta_b c)/\omega_{cb}$, and (b) the normalized growth rate ω_i/ω_{cb} versus kc/ω_{cb} obtained from Eq.(36) for $\beta_\perp = 0.5$, $\beta_b = 0.2$ and $s = 0.05$. The solid curves in Fig. 1(a) correspond to stable oscillations with $Im\omega = 0$, and the broken curves correspond to unstable modes with $Im\omega = \omega_i > 0$.

Fig. 2. Plots of (a) the normalized Doppler-shifted real frequency $(\omega_r - k\beta_b c)/\omega_{cb}$, and (b) the normalized growth rate ω_i/ω_{cb} versus kc/ω_{cb} obtained from the reference dispersion relation (RDR) in Eq.(39) for $\beta_\perp = 0.5$, $\beta_b = 0.2$ and $s = 0.05$. The solid curves in Fig. 2(a) correspond to stable oscillations with $Im\omega = 0$, and the broken curves correspond to the real frequency of the unstable modes with $Im\omega = \omega_i > 0$.

Fig. 3. Plots of (a) the normalized Doppler-shifted real frequency $(\omega_r - k\beta_b c)/\omega_{cb}$, and (b) the normalized growth rate ω_i/ω_{cb} versus kc/ω_{cb} obtained from Eq.(36) for the high frequency resonance (HFR) mode for $\beta_\perp = 0.5$, $\beta_b = 0.2$ and several values of s. The solid and dashed curves correspond to the fast- and slow-wave branches, respectively.

Fig. 4. Plots of (a) the normalized Doppler-shifted real frequency and (b) the normalized growth rate versus kc/ω_{cb} obtained from Eq.(36) for the low frequency resonance (LFR) mode for $\beta_\perp = 0.5$, $\beta_b = 0.2$ and several values of s. The solid and dashed curves correspond to the fast- and slow-wave branches, respectively.

Fig. 5. Schematic plot of the function $h^2(\zeta^2,s)$ versus ζ^2 assuming $\gamma_z^2\beta_\perp^2 < 2$ [Eq.(54)].

Fig. 6. Plots of the normalized maximum growth rate ω_i/ω_{cb} versus s for $\beta_\perp = 0.5$, $\beta_b = 0.2$ and $\zeta = 0$. The dashed, solid, and dotted curves are obtained from Eqs.(62), (36), and (39), respectively.

Fig. 7. Plots of the normalized bandwidth $c(\Delta k)/\omega_{cb}$ versus s for $\beta_\perp = 0.5$, and $\beta_b = 0.2$. The solid, dashed, and dotted curves are obtained from Eqs.(36), (70), and (39), respectively.

Fig. 8. Plots of the normalized frequency shift $\delta\omega_r/\omega_{cb}$ versus s for $\beta_\perp = 0.5$, $\beta_b = 0.2$, and $\zeta = 0$ corresponding to the maximum growth rate. The solid and dotted curves are obtained from Eqs.(36) and (39), respectively. The solution to Eq.(72) for $\zeta = 0$ is the straight line $\delta\omega_r = 0$.

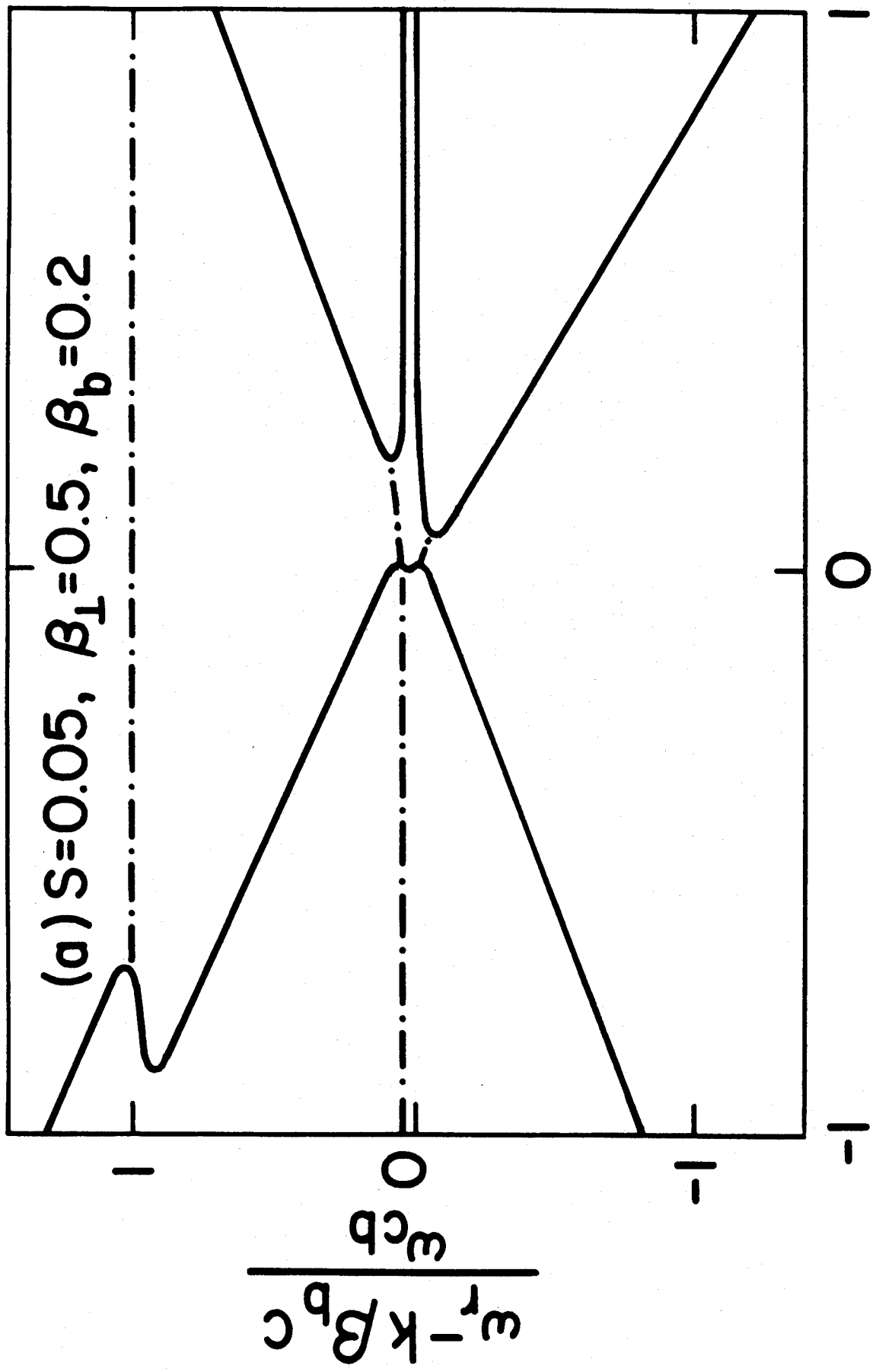
(a) S=0.05, $\beta_\perp$=0.5, β_b=0.2
$\frac{\omega_r - k\beta_b c}{\omega_{cb}}$
1
0
-1
1
0
-1
kc/ω_{cb}

Fig. 1(a)

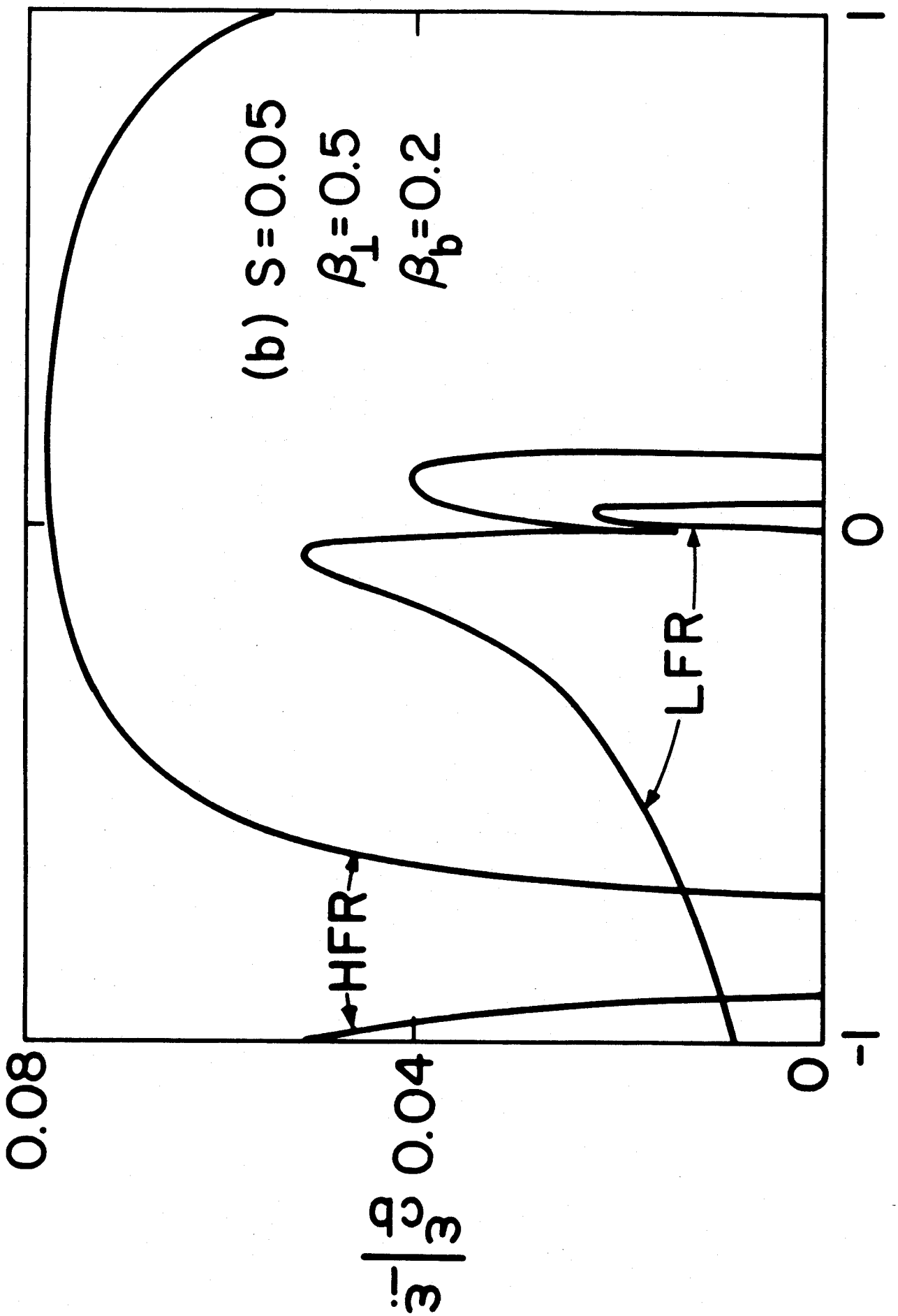
(b) S=0.05
$\beta_\perp$=0.5
β_b=0.2
HFR
LFR
0.08
0.04
0
$\frac{\omega_i}{\omega_{cb}}$
1
0
-1
kc/ω_{cb}

Fig. 1 (b)

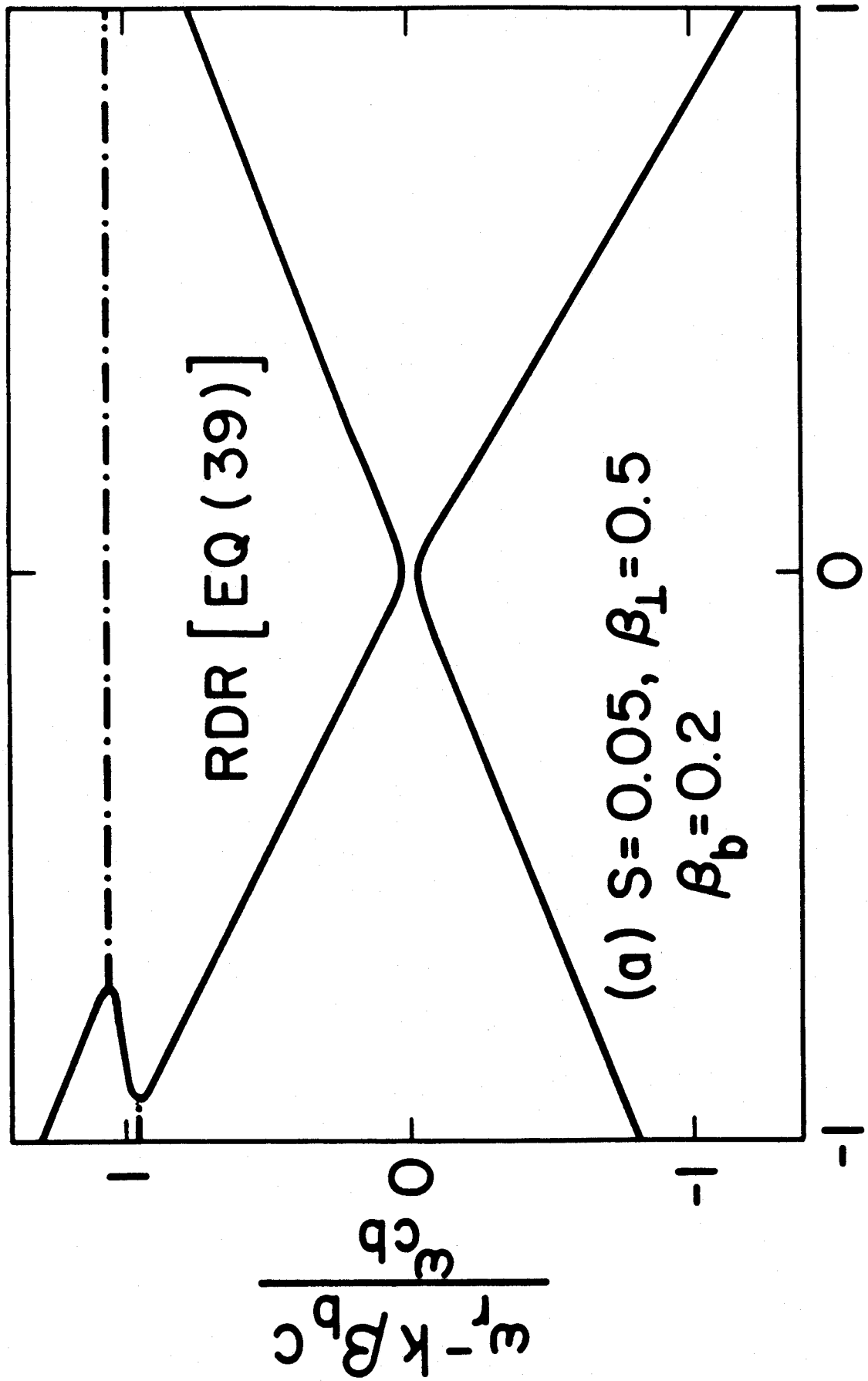
RDR [EQ (39)]
(a) S=0.05, $\beta_\perp$=0.5
β_b=0.2
kc/ω_{cb}
$\frac{\omega_r - k\beta_b c}{\omega_{cb}}$
1
0
-1
1
0
-1

Fig. 2(a)

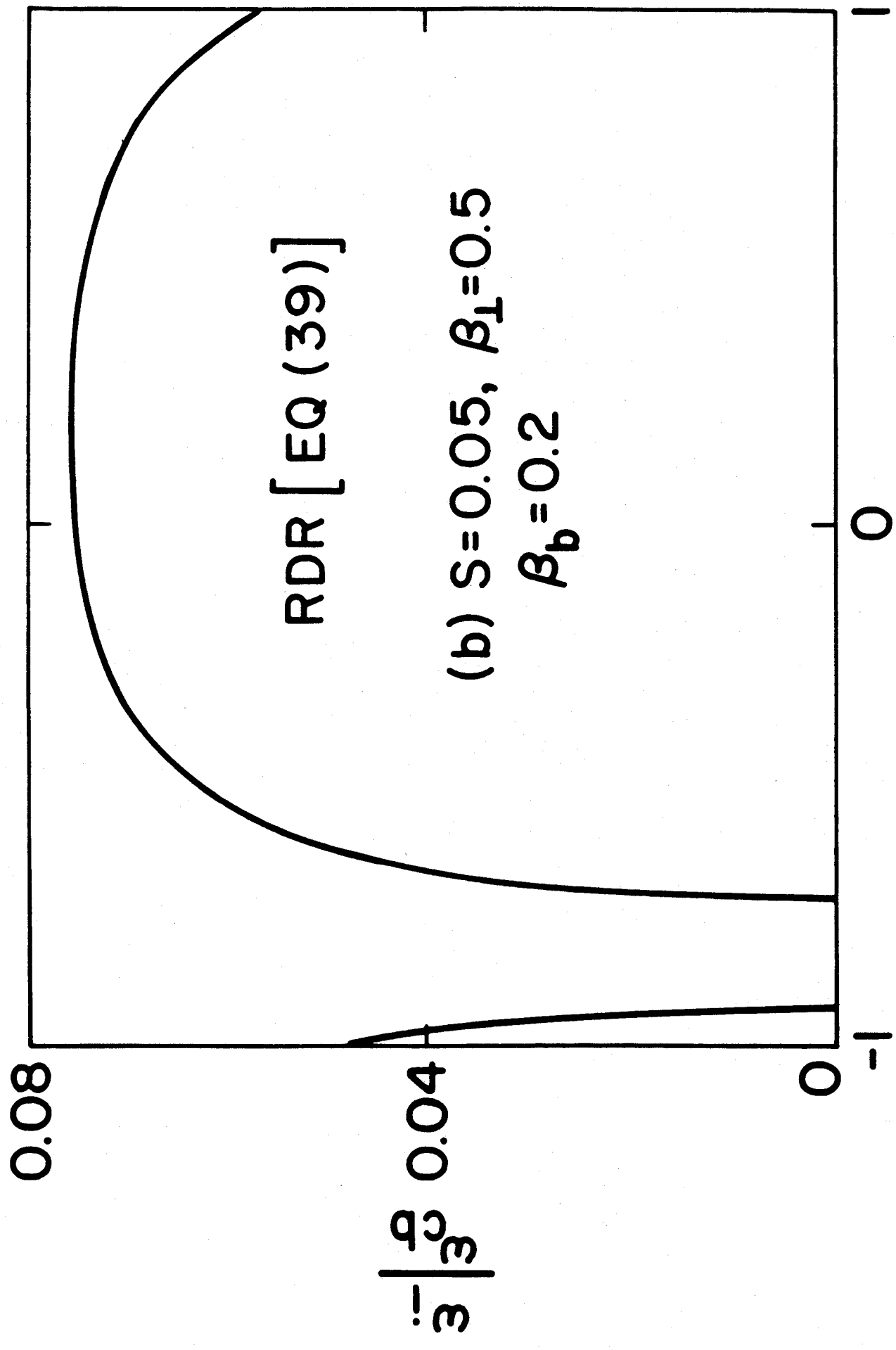
RDR [EQ (39)]
(b) S=0.05, $\beta_\perp$=0.5
β_b=0.2
$|q_3^3/i_3^!|$
0.08
0.04
0
-1
0
1
kc/ω_{cb}

Fig. 2(b)

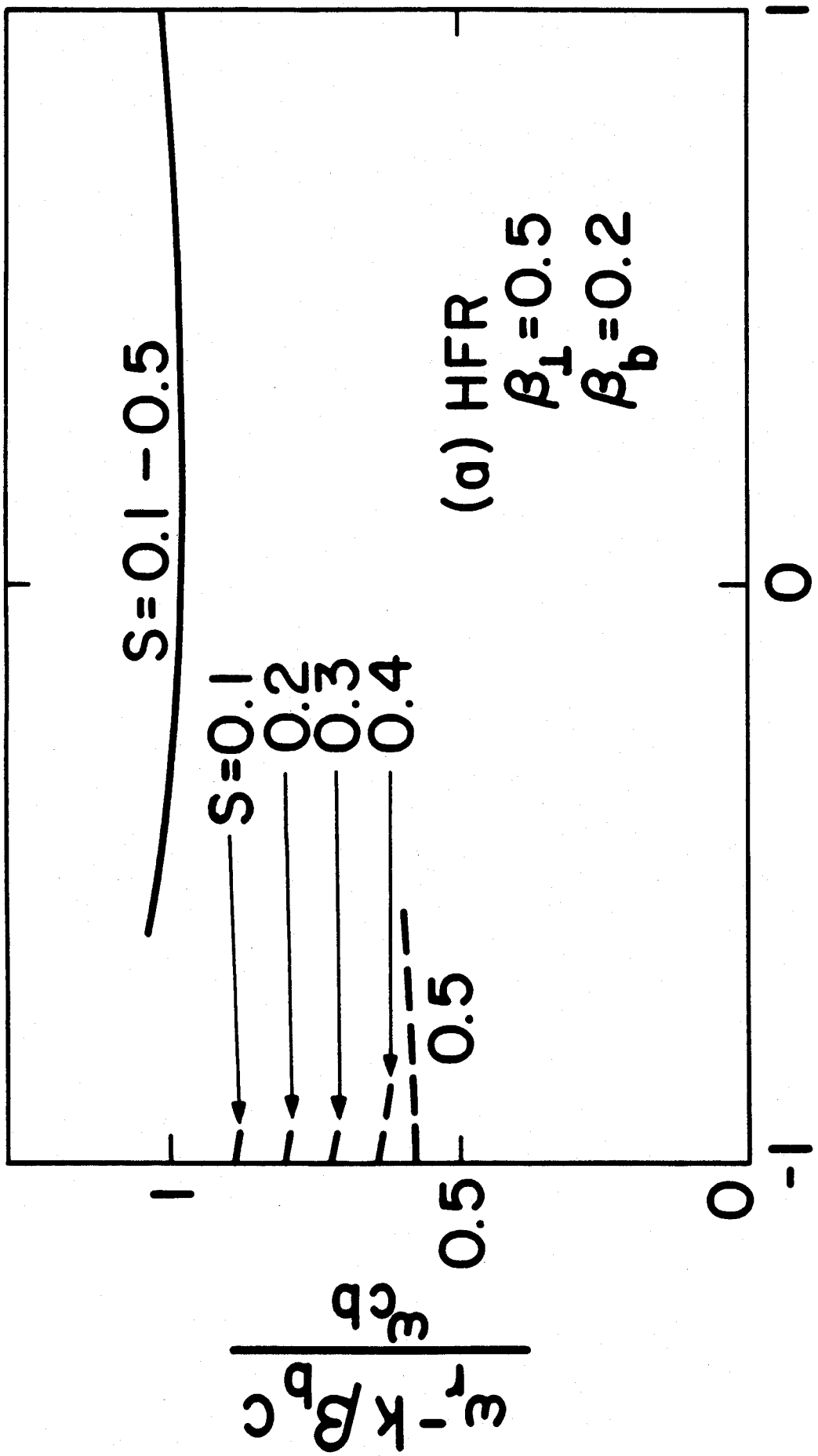
(a) HFR
$\beta_\perp$=0.5
β_b=0.2
S=0.1 – 0.5
S=0.1
0.2
0.3
0.4
0.5
kc/ω_{cb}
$\frac{\omega_r - k\beta_b c}{\omega_{cb}}$
1
0.5
0
-1

Fig. 3(a)

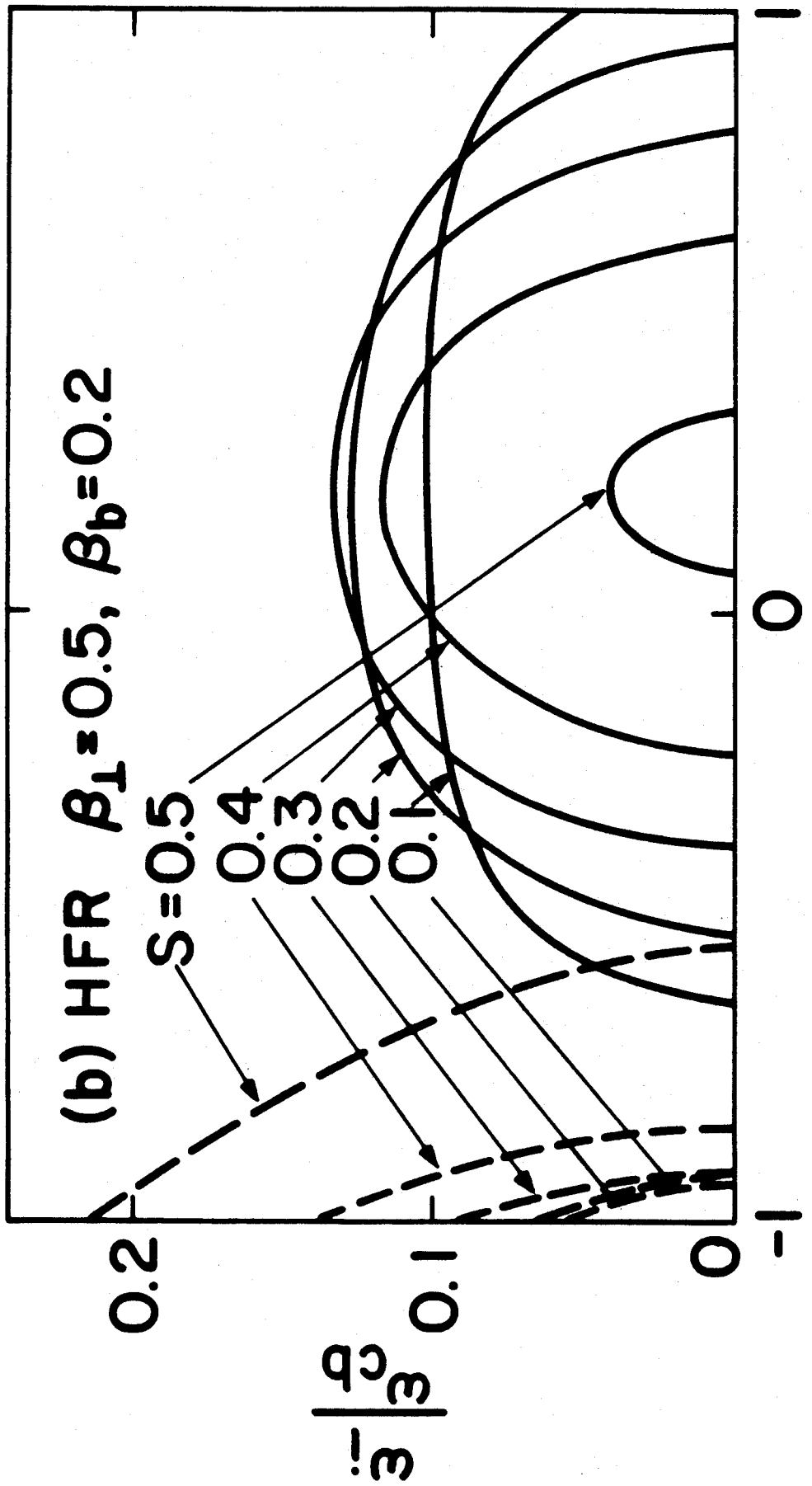
(b) HFR $\beta_\perp$=0.5, β_b=0.2
S=0.5
0.4
0.3
0.2
0.1
0.2
0.1
0
$\frac{\omega_r}{\omega_{cb}}$
-1
0
1
kc/ω_{cb}

Fig. 3(b)

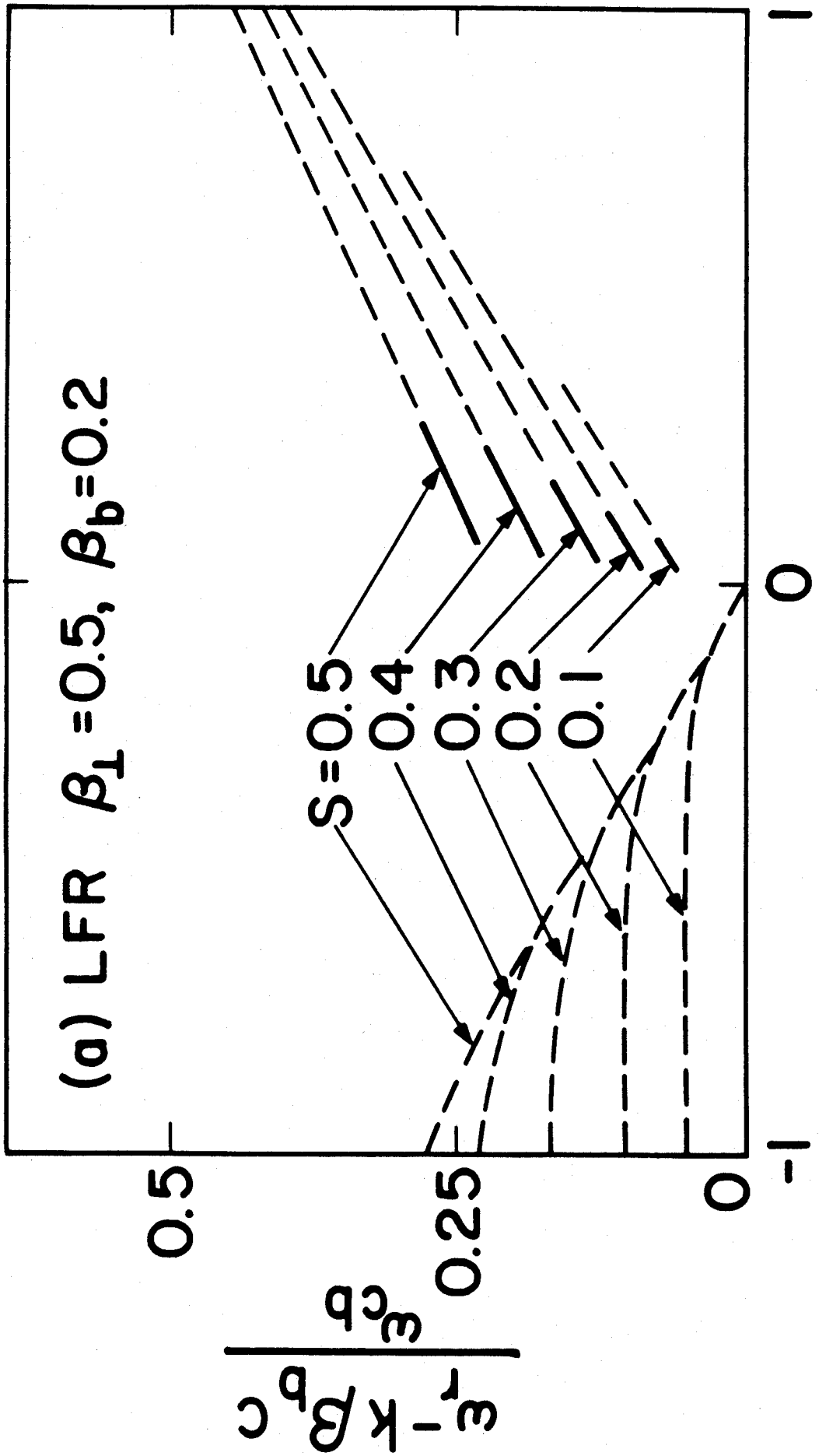
(a) LFR $\beta_\perp$=0.5, β_b=0.2
S=0.5
0.4
0.3
0.2
0.1
0.5
0.25
0
-1
1
0
kc/ω_{cb}
$\frac{\varepsilon_r - k\beta_b c}{\omega_{cb}}$

Fig. 4(a)

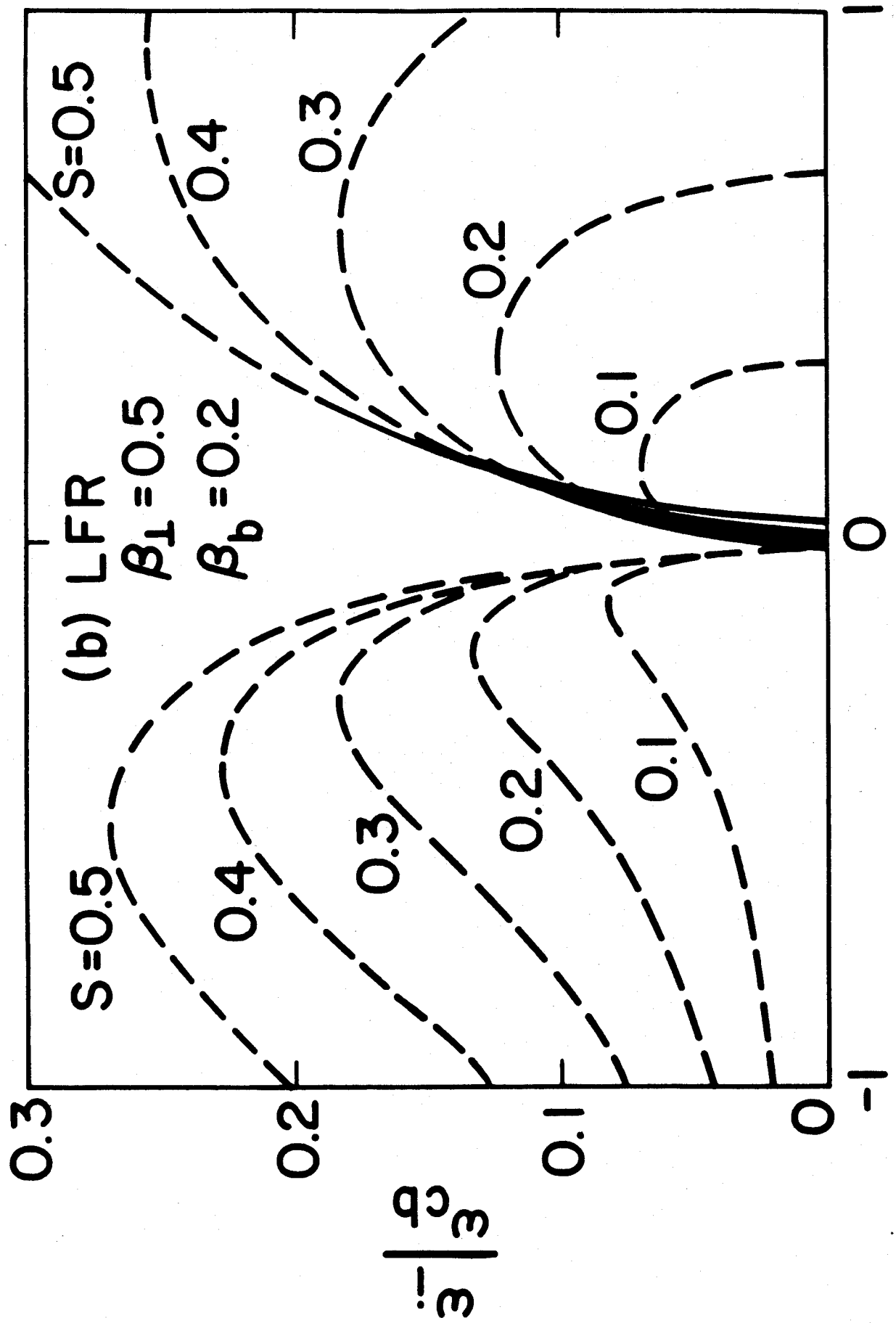
(b) LFR
$\beta_\perp$=0.5
β_b=0.2
S=0.5
0.4
0.3
0.2
0.1
S=0.5
0.4
0.3
0.2
0.1
0.3
0.2
0.1
0
-1
1
0
kc/ω_{cb}
$\frac{\omega_r}{\omega_{cb}}$

Fig. 4(b)

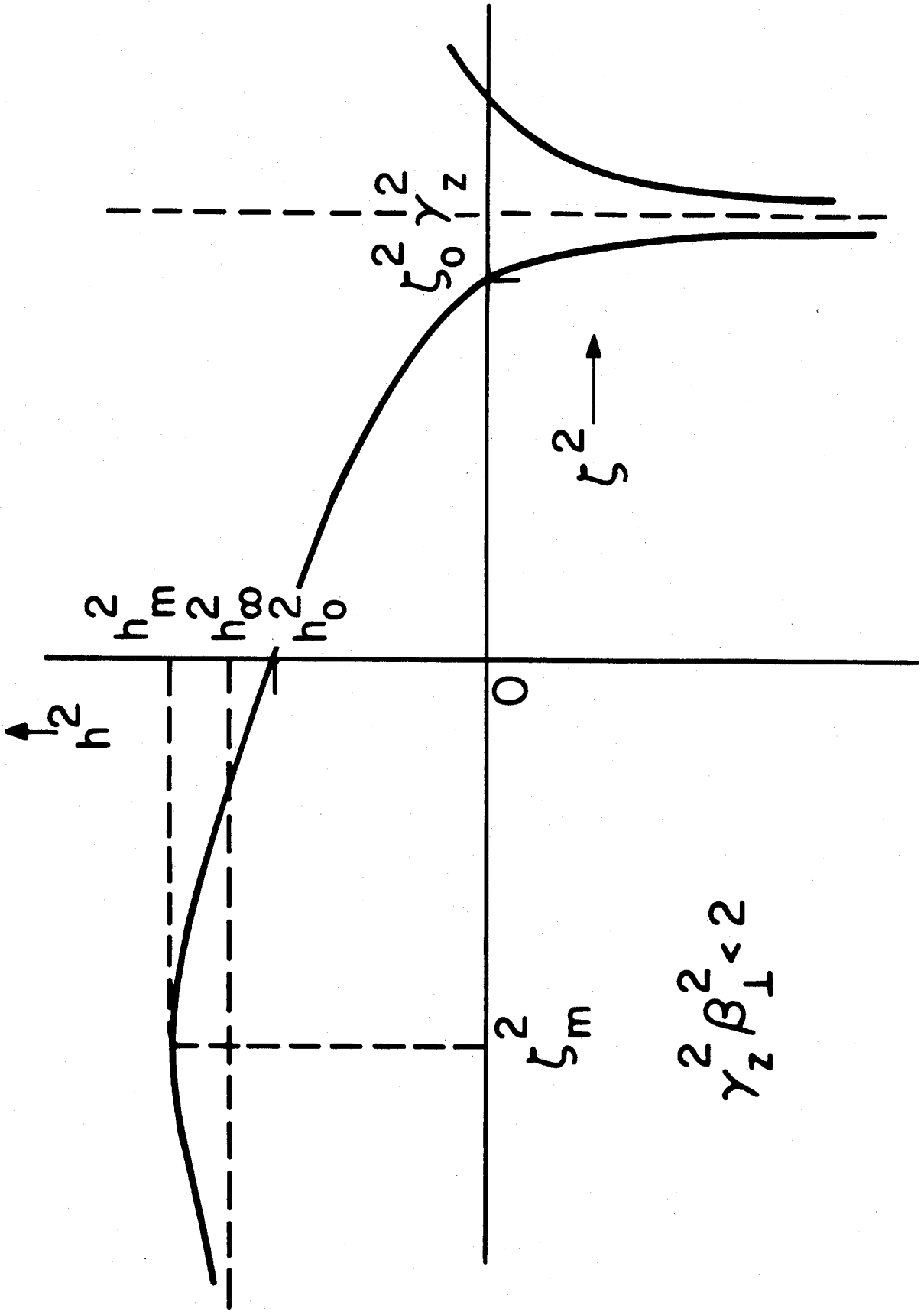
$\zeta_0^2 \gamma_z^2$
ζ^2
h_m^2
h_8^2
h_o^2
h^2
0
ζ_m^2
$\gamma_z^2 \beta_\perp^2 < 2$

Fig. 5

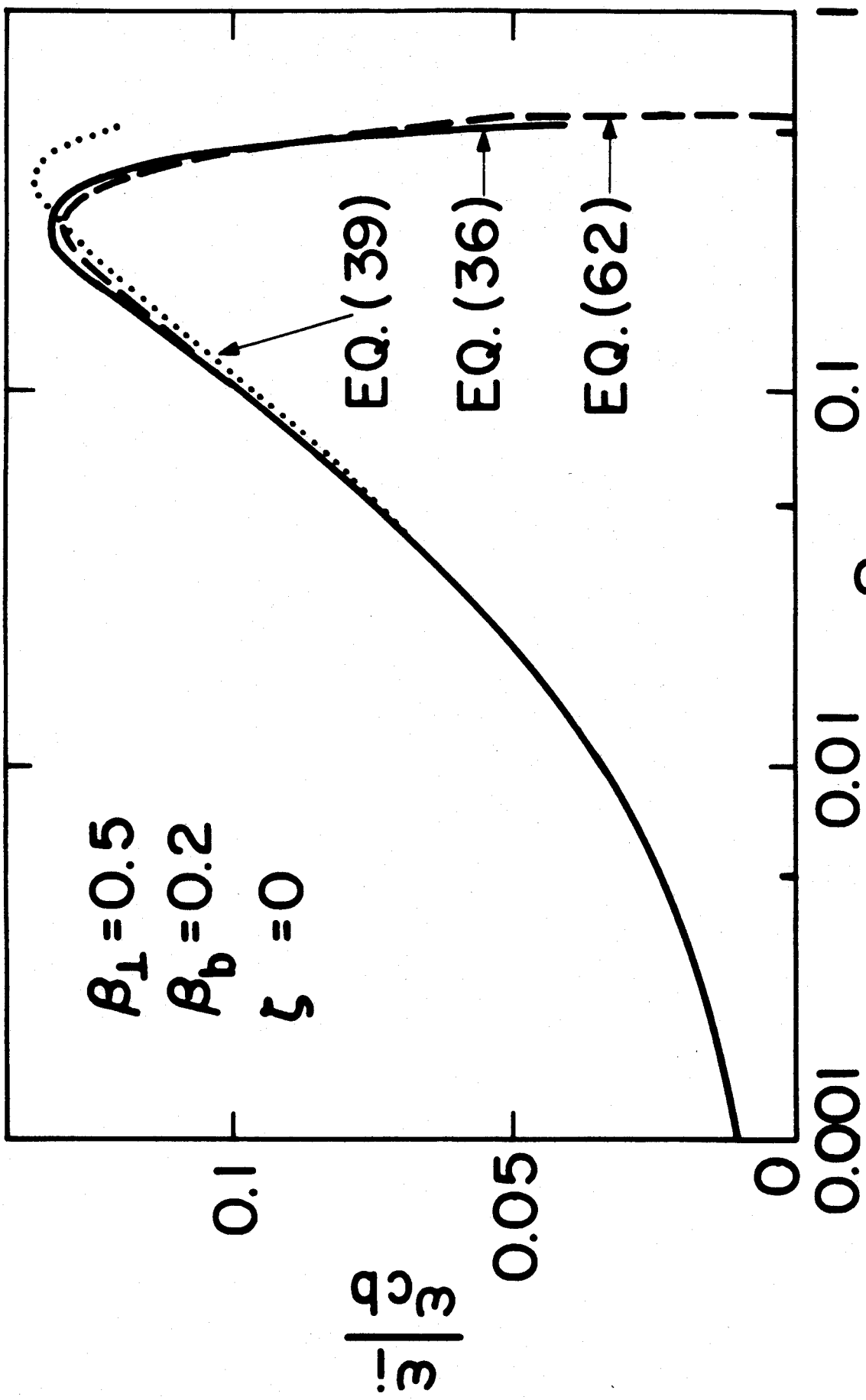
$\frac{\omega_i}{\omega_{cb}}$
0.1
0.05
0
0.0001
0.001
0.01
0.1
1
S
$\beta_\perp = 0.5$
$\beta_b = 0.2$
$\zeta = 0$
EQ. (39)
EQ. (36)
EQ. (62)

Fig. 6

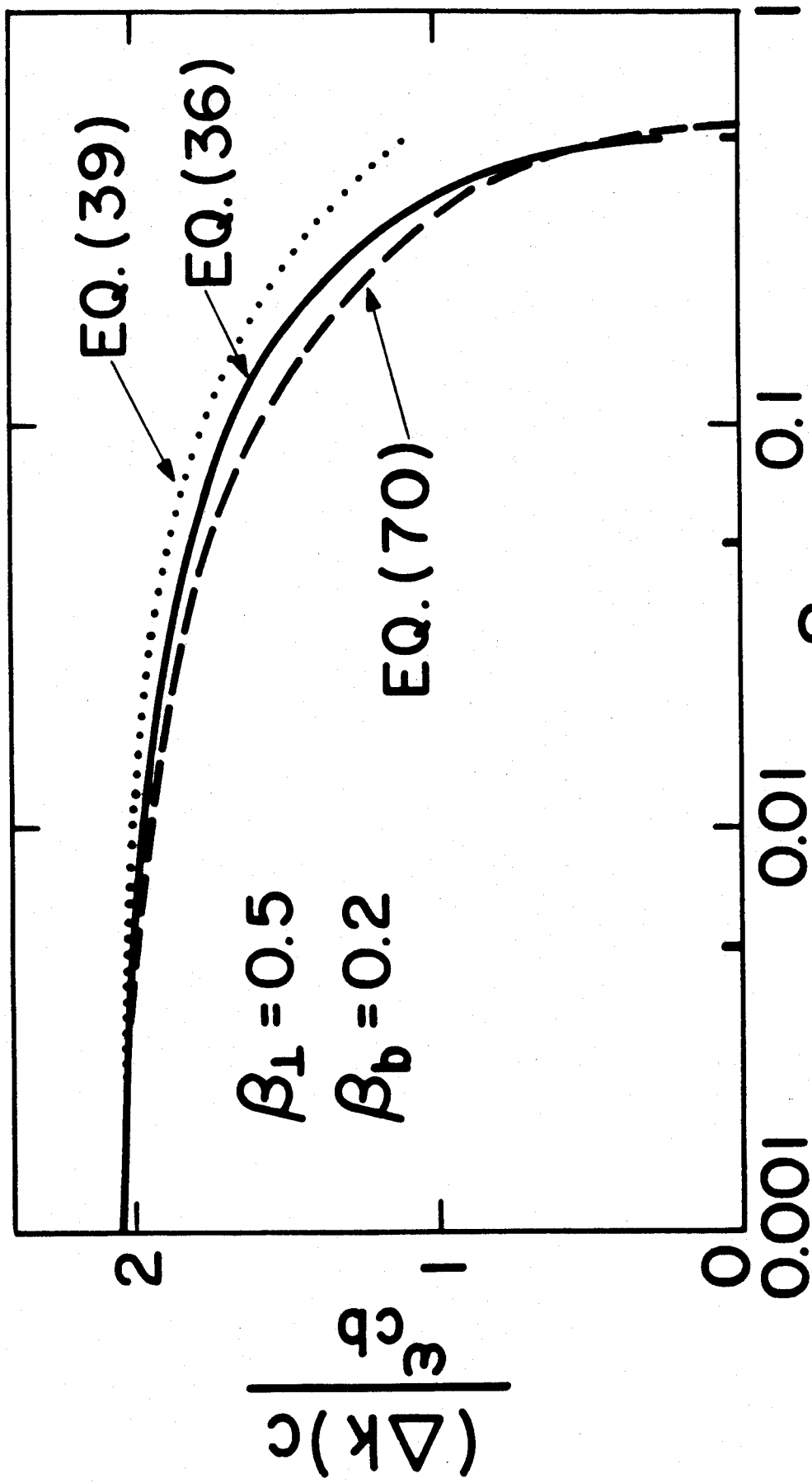
EQ. (39)
EQ. (36)
EQ. (70)
$\beta_\perp = 0.5$
$\beta_b = 0.2$
2
1
0
0.001
0.01
0.1
1
S
$\frac{\omega_{cb}}{(\Delta k)c}$

Fig. 7

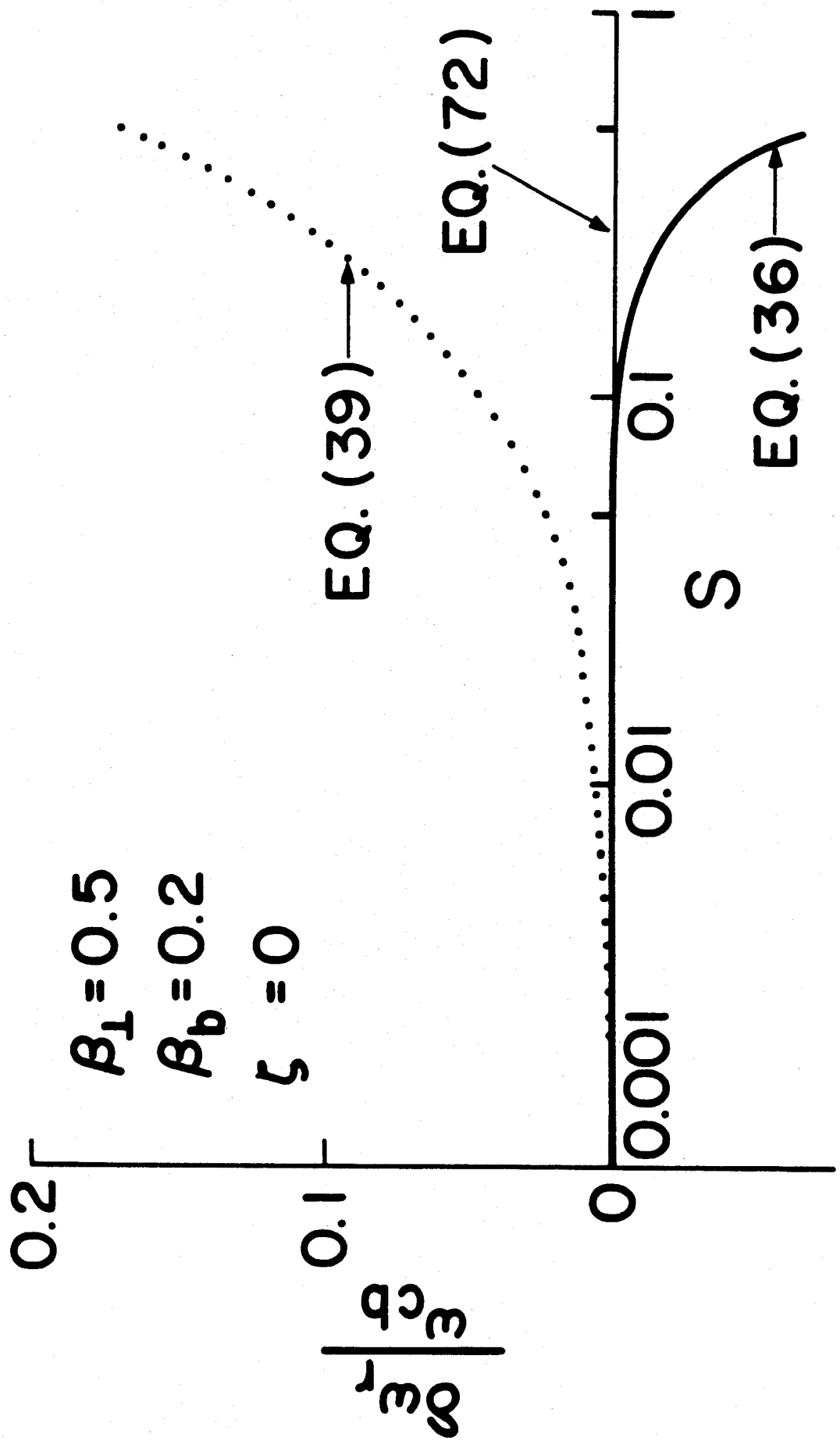
β_T=0.5
β_b=0.2
ζ =0
EQ. (39)
EQ. (72)
EQ. (36)
S
0.001
0.01
0.1
1
0
0.1
0.2
$\frac{\omega_{cb}}{\omega_T}$

Fig. 8